Fracture of Ceramics**

By *Robert Danzer, Tanja Lube,* * *Peter Supancic* and *Rajiv Damani*

The paper reviews the current state of art of the fracture of brittle ceramic materials. Typical loading situations (thermal shock, contact damage) are analysed and the resulting fracture modes are discussed. In focus of the paper are the brittle fracture and the resulting probabilistic aspects. The delayed failure of brittle materials (sub critical crack growth and cyclic fatigue) is also discussed.

Fracture of Ceramics

Robert Danzer*, Tanja Lube*,[1], Peter Supancic*, Rajiv Damani[#]

*Institut für Struktur- und Funktionskeramik, Montanuniversität Leoben, 8700 Leoben, Austria
[#]Sulzer Innotec 1551, Sulzer Markets and Technology Ltd., CH-8404 Winterthur, Switzerland

1.   Introduction

Ceramic materials have a large fraction of ionic or covalent bonds. This results in some special behaviour and consequently some special problems with their reliable use in engineering. In the temperature range of technical interest dislocations are relatively immobile and dislocation induced plasticity is almost completely absent in ceramics [1-3]. This is the basis for their high hardness and inherent brittleness. Typical values for the fracture toughness of ceramics are in the range from 1 to 10 MPa·m$^{1/2}$ and the total fracture strain is commonly less than a few parts per thousand [4].

In general the plastic yield stress is a factor of 10 higher than the tensile strength [1-4]. Therefore, local stress concentrations can not be relaxed by yield. This implies the need for careful design of highly loaded ceramic parts, for more precise tolerances (compared to parts made of metals or polymers) and for very careful handling of those parts, both in production and in application. It also entails the need for extremely careful stress analysis. In the region of load transfer into the component a steep stress gradient may occur and dangerous tensile stresses even exist around compressive contact zones (a prominent example of the damaging action of these tensile stresses are Hertzian cone cracks, which can frequently be found in impacted surfaces [3, 5]). Other significant mechanical stresses, which are not accounted for by an overly simplistic mechanical analysis, may result from thermal mismatch strains.

Mechanical testing is more complicated for ceramics than for ductile materials since problems arising from any misalignment of specimens can become severe. They cannot be balanced by small amounts of plastic deformation and this makes specimens with complicated shape or the use of very sophisticated testing jigs necessary. For the hard and brittle ceramics, machining of specimens is expensive and time consuming. Standardisation for mechanical testing procedures began around 30 years ago at national level. In the last ten years serious effort on internationalisation has also been made and the first international standard (ISO 14704: determination of bending strength at room temperature [6, 7]) was published in the year 2000. However, the process is far from complete. Even for such an important property like fracture toughness consensus on an appropriate testing procedure (i.e. an international standard) has not yet been achieved [8-10, 7, 11, 12]. In light of this background, it is not surprising that good and comparable data, such as that needed for appropriate material selection, is missing for most ceramic materials [13].

In ceramics, fracture starts in general from small flaws, which are discontinuities in the microstructure and which, for simplicity, can be assumed to be small cracks distributed in the surface or volume. Strength then depends on the size of the largest (or critical) defect in a specimen, and this varies from component to component [1-4, 14]. The strength of a ceramic material cannot, therefore, be described uniquely by a single number; a strength distribution function is necessary and a large number of specimens is required to characterise this. Design with ceramics has to be approached statistically. A structure is not safe or unsafe, but it has a certain probability of failure or survival. A failure probability of zero is equivalent to the certainty that the component contains no defect larger than a given size. The critical defect size for typical

---

[1] corresponding author: tanja.lube@unileoben.ac.at, tel.: +43(0)3842 402-4111, fax: +43(0)3842 402-4102

design loads in technical ceramic components is around 100 μm or smaller and is therefore too small to be reliably found by non-destructive testing techniques. Proof testing is usual for components needing high reliability.

Taking all these problems into account it becomes clear that their high brittleness and insignificant ductility impedes the wider use of ceramics as advanced technical materials. A detailed understanding of the damage mechanisms and fracture processes is necessary to make the safe and reliable application of ceramic components possible.

2. Appearance of Failure and Typical Failure Modes

Fracture of ceramic components depends on many factors, e.g. the chemistry and microstructure of the material and the resulting materials properties (e.g. toughness, R-curve behaviour, etc.). The macroscopic appearance of fracture is, however, primarily influenced by the type of loading of the component and the resulting stress field.

(a)

(b)

(c)
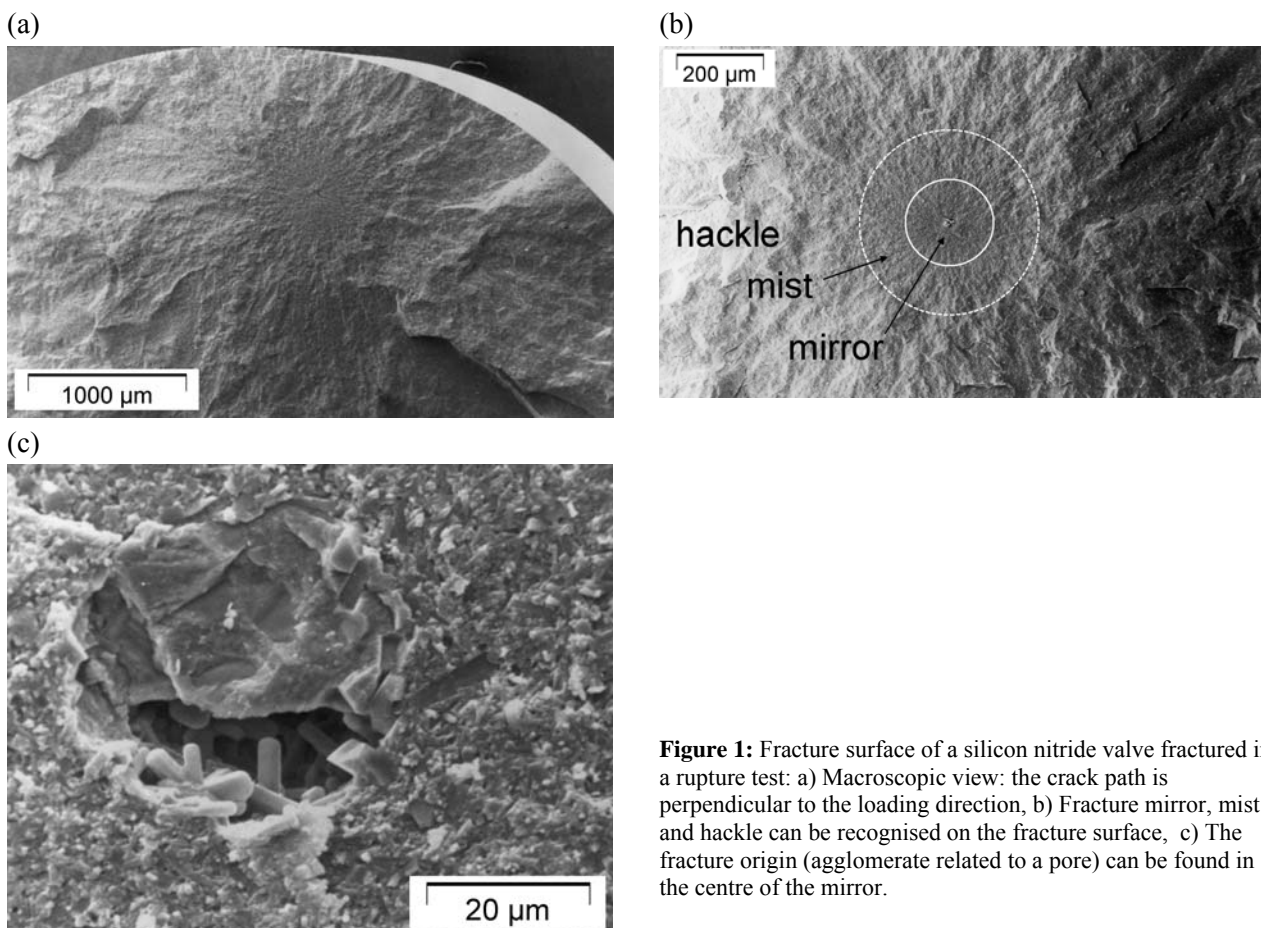
Figure 1: Fracture surface of a silicon nitride valve fractured in a rupture test: a) Macroscopic view: the crack path is perpendicular to the loading direction, b) Fracture mirror, mist and hackle can be recognised on the fracture surface, c) The fracture origin (agglomerate related to a pore) can be found in the centre of the mirror.

At low and ambient temperatures fracture of ceramics is always brittle. It is triggered by the normal tensile stresses in the component. An example of a typical fracture surface is given in **Figure 1**, which shows the forced rupture of a silicon nitride valve tested in a tensile test [15]. The fracture path is almost perpendicular

3

to the direction of loading (i.e., to the first principal stress). No signs of plastic deformation can be detected. The fracture origin is surrounded by a smooth area, called the fracture mirror, and by rougher regions referred to as mist and hackle [16-19]. In this case, the fracture origin is an agglomerate related to a pore. Such features are very common in brittle fracture of ceramic materials: the fracture origin is a critical flaw which behaves like a crack; the crack path is perpendicular to the first principal stress (at least at the beginning of crack extension) and the fracture origin is surrounded by mirror, mist and hackle. The size of the fracture origin, mirror, and mist respectively are found to be proportional to σ^{-2}, σ being the stress in an uncracked body at the position of the origin of fracture [16]. Mirror constants can be found in literature [17, 18, 20].

This type of fracture can be found in both very large and very small systems, e.g. in fractured natural rocks, in tested specimens of advanced ceramic materials, and even in broken ceramic fibres. Fracture mirror size measurements can be used for post mortem determination of the failure stress in components [21].

(a)

(b)

1000 µm
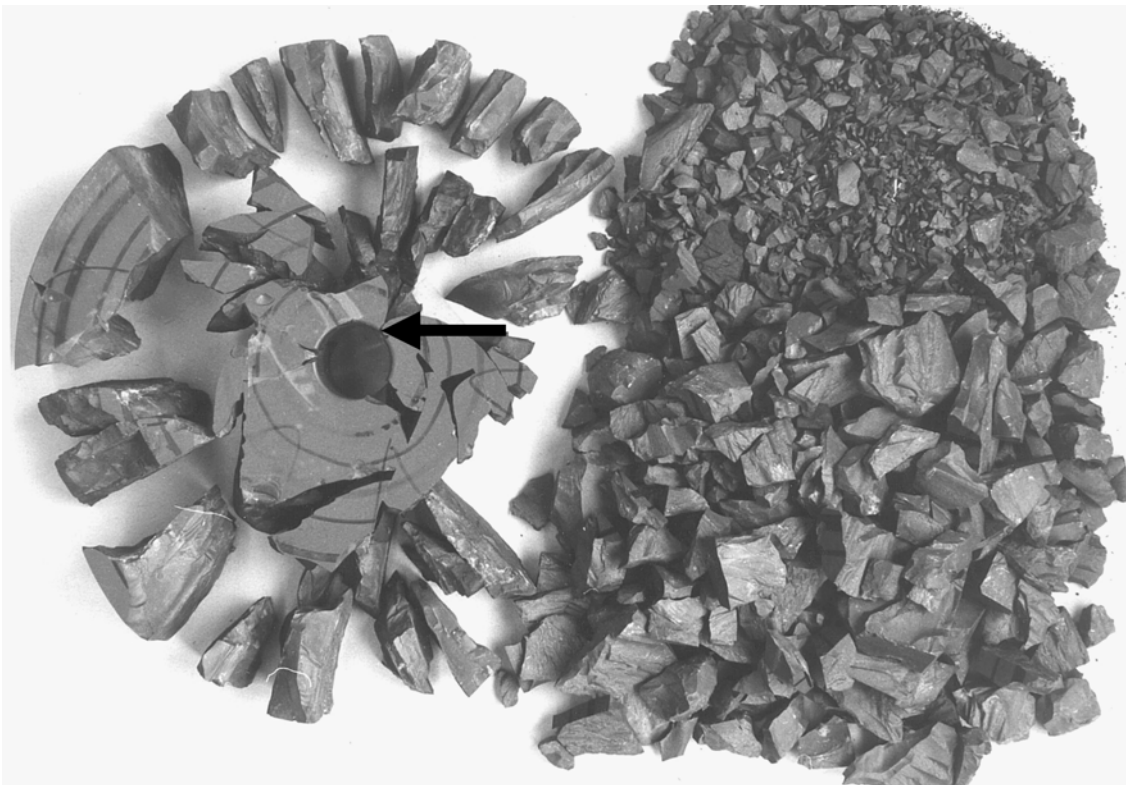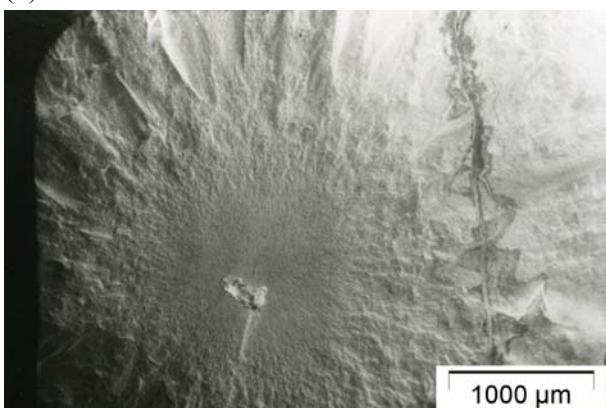
Figure 2: Turbine rotor made of silicon nitride ruptured in a spin test: a) fractured rotor (the location of the fracture origin is indicated by an arrow) and b) fracture origin. [22, 23].

Compared to failure in a tensile test, the failure of components in operation can be much more complex. The stress field is generally not uniaxial, which may cause an intricate crack path. In many cases secondary damage may confuse the initial picture. **Figure 2** shows the remnants of a turbine rotor fractured in a spin test [22, 23]. The fracture origin was again identified as a flaw in the microstructure.

Many modes of failure in operation exist. These are typically defined by the mode of loading and each results in a characteristic macroscopic fracture appearance. Nevertheless, a huge fraction of in–service failures can be traced back to just two groups of failure modes: i) thermal shock and ii) contact loading. These are described in more detail in the following.

2.1. Thermal shock failure

Thermal shock (or thermos shock) failure is a very prominent failure mode in ceramics. From the fractographic experience of the authors it is apparent that more than a third of all rejections of ceramic components are caused by thermal shock.

Thermal shock occurs when rapid temperature changes cause temperature differences and thermal strains in the component [4, 19, 24-26]. If these strains are constrained thermal stresses which may cause crack propagation and failure can arise. The shape of the stress field depends on the boundary conditions. The most important example for thermal shock is cooling shock (e.g. due to quenching of a hot part). During cooling, heat is transferred via the surface of a component into the environment and the surface cools down. As a result, material in the surface region attempts to shrink. This, however, is constraint by the interior of the material, which is still at a higher temperature. Such constraint causes tensile stresses in the surface region, analogous to those in a hypothetical elastic layer stretched over the component. The interior of the body is in compression. If tensile stresses exceed certain critical values, damage occurs resulting in characteristic crack patterns. Examples of thermal shock damage in samples and components [26, 27] are shown in **Figure 3** and **Figure 4.**

(a)   (b)
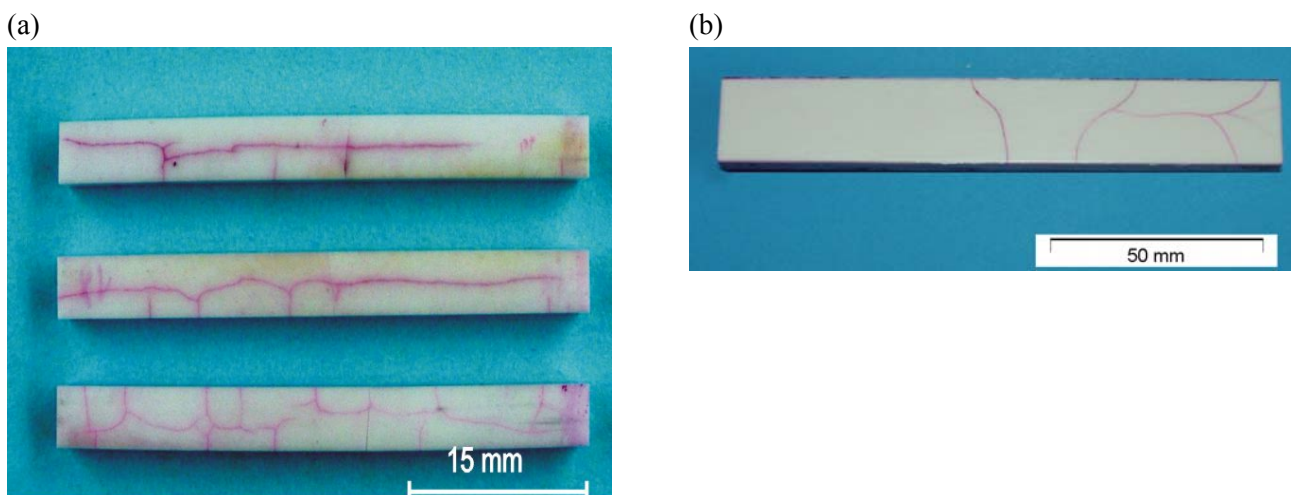
Figure 3: Thermal shock cracks in alumina ceramics a) in quenched specimens and b) in a paper machine foil after severe operation. In this case the thermal shock was caused by water cooling after frictional heating. The cracks are highlighted by a dye penetrant**.**

Thermal shock cracks develop if stresses become locally supercritical. The growth of such cracks reduces the tensile stress in their surrounding and thus the driving force for further extension. Consequently, crack

propagation may stop. The number of cracks increases with the severity of the shock. Whereas thermoshock cracks typically run perpendicular to edges, at flat surfaces (where biaxial stress states exist) they tend to form networks, which look quite similar to the mud cracking patterns observed in dried-up marshes. The growth direction of cracks is opposite to that of heat flow. Due to their characteristic appearance, thermal shock cracks can in general be recognised by simple optical inspection of the damaged component.

(a)

(b)
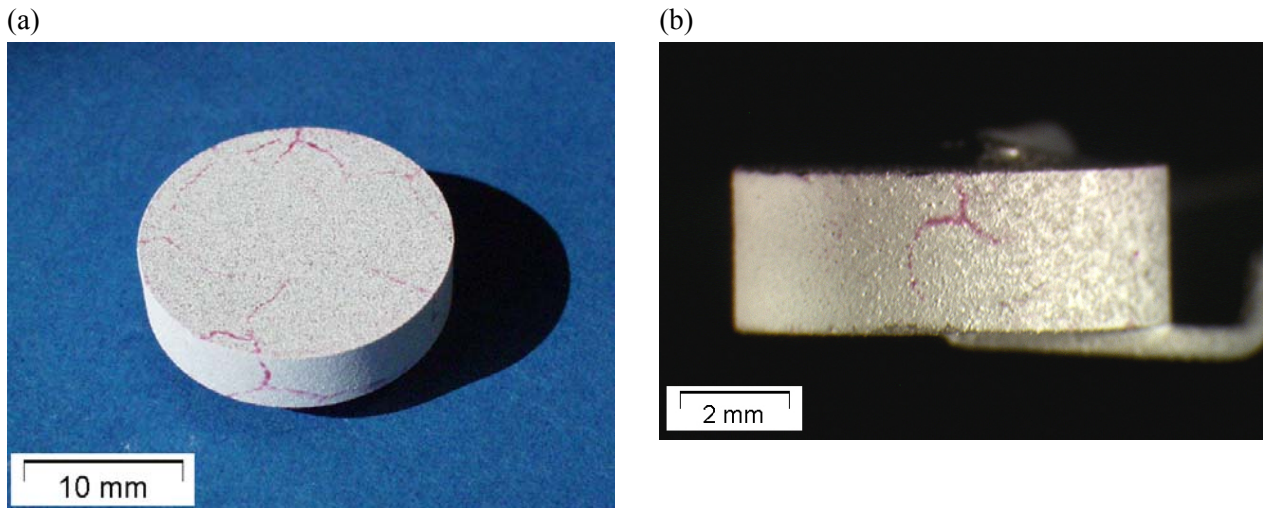
Figure 4: Thermal shock cracks in PTC-ceramics a) in a quenched specimen and b) in a PTC resistor after soldering. The reason for the crack formation was an inappropriate handling of the component during soldering. The component has been taken out of the furnace by a cold pair of metal pliers. The cracks are marked by a dye penetrant.

2.2. Contact failure

Loading contact of hard surfaces, e.g., by static or dynamic impingement of bodies, can lead to cracking if stresses exceed critical values. Such damage typically occurs in one of two modes: local area loading or 'blunt contact' or point loading or 'sharp contact'.

Blunt contact is a classic scenario and was comprehensively treated by Hertz [5] who modelled it as the contact between a sphere and a flat surface. When the surfaces of two such bodies touch, they deform elastically and form a circular contact area. Under this contact area compressive stresses arise whose amplitude is a function of the elasticity of the two surfaces and which increase with both the applied load and decreasing radius of the sphere. The contact zone is encircled by a narrow ring shaped region where significant tensile stresses occur. These have a maximum amplitude of about ¼ of the mean contact pressure [28]. If the tensile stresses locally exceed some critical value a ring shaped crack (Hertzian ring crack) is formed. Since tensile stresses, and therefore the driving force for crack propagation, steeply decrease below a surface, Hertzian ring cracks generally do not penetrate deeply. (However, further increases in loading will cause such cracks to extend further at an oblique angle of about 22° from the indented surface to form a cone shaped crack [28]). Such damage is typically caused and studied by means of blunt indentation techniques such as Brinell hardness.

Hertzian cracks are often caused in service due to inappropriate handling or due to localised overload. They may cause immediate (catastrophic) failure or may provide the origin for some sort of delayed failure.

Figure 5a and **Figure 5b** show a Hertzian ring crack in the surface of a silicon nitride specimen and cracks caused by contact damage in a silicon nitride roll for the rolling of high alloyed steel wires [29]. It is obvious that the reason for the cracks is similar in both cases. In the case of the roll, the shape of the working groove

6

and the contact area of the wire with the groove had significant influence on the shape of the crack [30]. Hertzian contact damage is also likely to occur in ceramic balls in ball bearings.

Sharp contact is a (pseudo) point loading situation and is well modelled by sharp indentation techniques like Vickers or Knoop hardness testing. Typically damage takes the form of severe plastic deformation beneath the point of contact and the formation of radial cracks at any sharp features such as the corners of the Vickers pyramid. The inelastic strains associated with plastic deformation produce high internal stresses which strongly influence the development of cracking and damage [28]. Lateral cracks may form below the plastically deformed region and extend parallel to the surface [31]. If these cracks intersect the radial cracks and the surface, large fragments (chips) of material may break away. In fact this is one of the most prolific mechanisms of wear in ceramics [32].

Figure 5c and **Figure 5d** show radial cracks and a break out caused by lateral cracks originating from a Vickers indent in the surface of silicon carbide and silicon nitride ceramics.
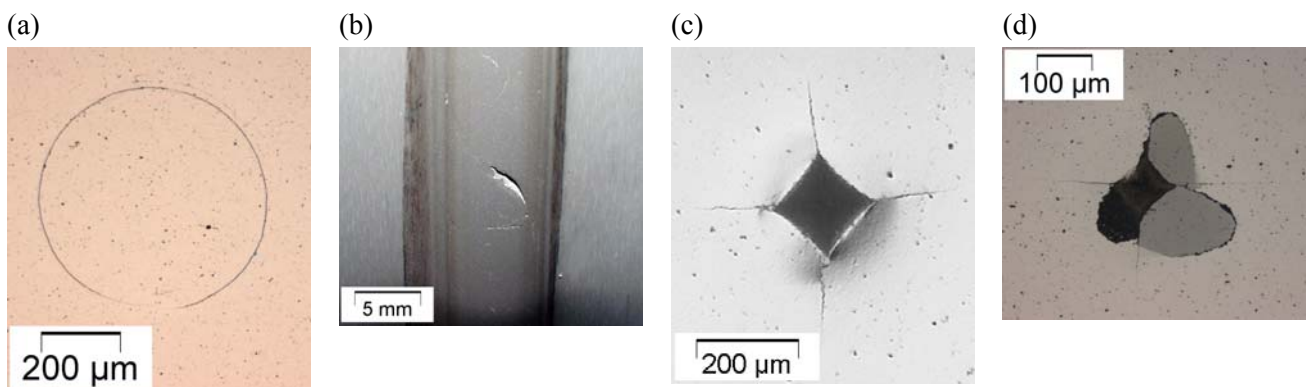

Figure 5:, Contact damage (cracks) in the surface of ceramics: a) and b) cracks caused by a blunt and c) and d) cracks caused by a sharp indenter. a) Hertzian ring crack in silicon carbide b) crack caused in operation by the rolling of high alloyed steel wires [30], c) radial cracks at the corners of a Vickers indent in silicon nitride and d) break out due to lateral cracks under a Vickers indent in silicon carbide.

An interesting variant of contact failure occurs if the contact is near an edge. The crack may not stop then and an edge flake breaks out [33-36]. Such edge flaking can often be observed in used ceramic components, e.g. in classical ceramic products such as marble steps, tableware and tiles [19], but is also seen in technical ceramic products like tool bits or guides for hot metal sheets in steel works and even in human teeth or tooth implants [37]. Examples of edge flakes are shown in **Figure 6**.

The contact damage discussed so far is caused by some kind of quasi static loading, but quite similar damage may occur from dynamic (impact) loading. For example a strike with a hammer having a rounded head can cause a Hertzian like ring crack at the surface of the component. A good every day example is the chipping and cracking in the windscreen of cars caused by the impact of grit and small stones.

Although frequently optically displeasing, contact damage does not always cause immediate failure, but may serve as the origin of some delayed failure caused by the subsequent steady or fast growth of cracks. The possible damage mechanisms will be discussed in section 3.
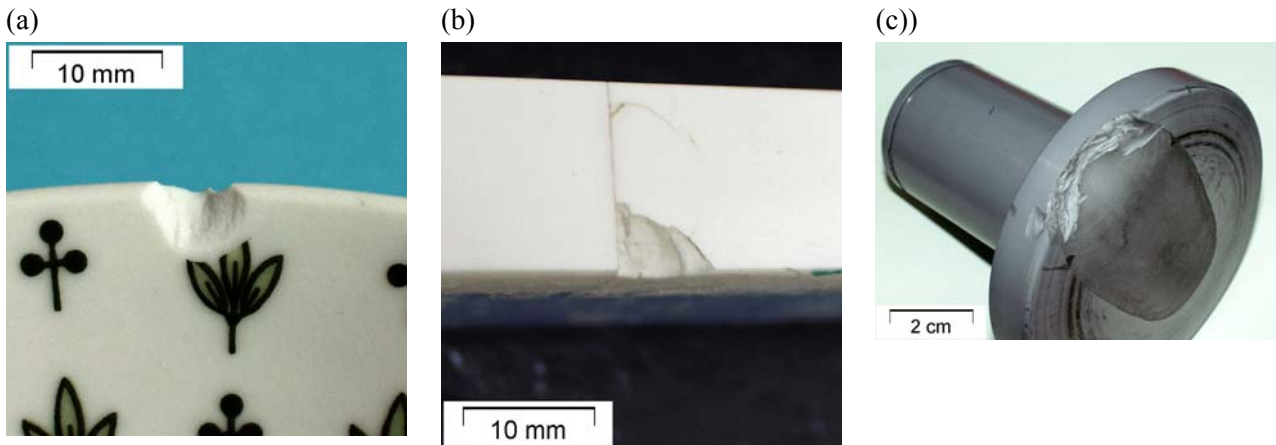
Figure 6: Examples of edge flakes in used ceramic components: a) in a plate, b) in a wear resistant alumina foil in a paper machine and c) in a silicon nitride guide for hot metal sheets in a steel work.

3.   A Short Overview of Damage Mechanisms

At room and ambient temperatures almost any fracture in ceramics is brittle. It occurs without any significant plastic deformation and the (elastic) failure strain is very small. Under load cracks may grow steadily until they almost reach the speed of sound and sudden catastrophic failure occurs. Several crack growth mechanisms exists, e.g. sub-critical crack growth, fatigue or corrosion. Ductile fracture only arises at very high temperatures (or at extremely slow deformation rates, but this is generally not relevant for technical applications) by creep. In the literature several classes of damage mechanism are identified [14]. These will be briefly described in the following:

- Sudden, catastrophic failure,
- sub-critical crack growth (SCCG),
- fatigue,
- creep,
- corrosion or oxidation.

Sudden, catastrophic failure is the most prominent damage mechanism in technical ceramics [1-4], and is inevitably the final active mechanism at failure. It is caused by the very quick growth of a single crack (the critical crack). The growth rate is so high, that crack arrest is almost not possible and fracture of the component almost immediately occurs when a critical load is applied. Flaws, which may serve as critical cracks, may, to give some examples, be generated during the production of the ceramic, by the machining of the component, by thermal shock, contact damage or corrosion and even by inadequate handling. Smaller cracks may grow to a critical size by SCCG, fatigue, creep, oxidation or corrosion (delayed failure). The time necessary for this growth determines the service life time of the component. Then sudden catastrophic failure occurs.

SCCG [38-41] is caused by the thermally activated breaking of bonds at the tip of a stressed crack [38]. It may be assisted by the corrosive action of some polar molecules (e.g. by water or water vapour) and is thus related to stress corrosion cracking as observed in metals [39, 40]. Some SCCG always precedes final catastrophic fracture in brittle materials, but if the load is applied very quickly, the contribution can be rather small. It can cause delayed failure of components (a long time after the application of the load) without any

plastic deformation of the ceramic material. Sometimes SCCG is also called fatigue (or static fatigue), but since it is not caused by cyclic loading, as in the case of fatigue in metals, this can be misleading. To avoid confusion, in the following the term fatigue will not be used in the context of SCCG.

For a long time cyclic fatigue was thought not to occur in linear elastic ceramics. Some 30 years ago, however, evidence of damage due to the alternating application of loads was also observed in advanced technical ceramics [42]. In the following, the term fatigue will be used exclusively to describe the damaging effects of cyclic loading.

In ceramics, fatigue crack growth is caused by repeated (cyclical) damage to microstructural elements, e.g., by the breaking of crack bridges during the crack closure part of a loading cycle [43, 44]. As with SCCG, fatigue may also be a reason for delayed failure and may precede the sudden catastrophic failure of a component.

Creep in ceramics is much less pronounced than in metals or polymers. The activation energy for creep of ceramics is much higher [45] and creep deformation and creep damage in ceramics therefore only occurs at very high temperatures [46]. (The activation energy approximately scales with the melting temperature [45] and the melting temperatures of most technical ceramics are high.) Creep damage is in general caused by the generation, growth and coalescence of pores. Creep damage is not localised like crack growth and may occur throughout a component [47]. The resulting final failure can be brittle as well as ductile depending on the acting stresses and temperatures. In most applications of technical ceramics creep does not occur (exceptions are some applications of refractories, e.g. as components in kilns and furnaces or as materials for lamps) and will therefore not be treated further here.

Corrosion, e.g., by oxidation, may cause serious damage in ceramics and can be an important wear mechanism [48]. If corrosion products are gaseous, severe loss of material can result [49]. Oxidation of grain boundaries may even cause the disintegration of a material [50]. Primarily with respect to fracture, corrosion and oxidation damage act as initiation sites for crack growth and consequent brittle fracture. To maintain brevity then, corrosion damage will also not be treated separately here.

In summary it can be stated that at low and ambient temperatures, fracture always occurs by brittle failure, which starts from crack like flaws in the micro structure. Brittle fracture can be preceded by some SCCG or fatigue crack growth [29]. The failure initiating flaws can either result from the production process of the material or come into existence due to inappropriate machining, handling or even by oxidation and corrosion. In the following sections these mechanisms and the consequences for mechanical design will be treated in more detail.

4.   Brittle Fracture

In ceramics, brittle fracture is controlled by the extension of small flaws which are dispersed in a material or component's surface and which behave like cracks. Flaws can arise from the production process, but also from handling and service. Examples for critical flaws were shown in **Figure 1** and **Figure 7**.

In this chapter brittle fracture is firstly discussed for the simple case of a uniaxial and homogeneous stress field (as in a tensile test) and for a single crack like flaw which is oriented perpendicular to the stress field (in so called mode I loading). These simple conditions are sufficient to explain the basic features of brittle fracture. Later the analysis will be extended to more complex and more general situations, i.e. multiple cracks, arbitrary orientation of cracks (mode II and mode III loading) and multi-axial stress fields.

4.1. Some Basics in Fracture Mechanics

Ultimately, fracture can only occur if all atomic bonds in a plane are pulled apart and break. The stress necessary to break a bond (the theoretical strength) is between $E/5$ and $E/20$, with E being the elastic modulus of the material [51]. Typical tensile stresses applied to highly loaded components are in the order of some $E/1000$ or even smaller and yet fracture of components still occurs. To explain this discrepancy it is necessary that some strong local stress concentrations exist. Flaws are locations of such stress concentrations. Let us discuss the action of flaws using the simple example of an elliptical hole in a uniaxial tensile loaded plate. At the tip of its major semi-axis (which is perpendicularly oriented to the stress direction) the stress concentration is [52]:

$$\sigma_n / \sigma = 1 + 2c/b \quad . \tag{1a}$$

σ is the applied far-field stress and σ_n is stress at the tip of the major semi-axis c of the ellipse. The minor semi-axis is b. So, for any circular hole, independently of its diameter, the stress concentration is three. It is obvious that the stress concentration may become very high, if the ellipse is extremely elongated, i.e. if $c \gg b$. For that case the equation can be approximated to give [51]

$$\sigma_n / \sigma \approx 2\sqrt{c/\rho} \quad , \tag{1b}$$

with ρ being the radius of curvature. Note how the stress concentration depends on the shape but not on the size of the notch and that, for $\rho \rightarrow 0$, the stress at the tip goes to infinity.

An elliptical hole must be extremely elongated to create the stress concentration necessary to reach the theoretical strength. To give a simple example, for an applied stress of $\sigma = E/1000$ the ratio of major to minor semi-axis has to be $c/b \approx 50$ ($c/\rho \geq 2500$) to create the stress concentration necessary to reach the theoretical strength at a notch tip: $\sigma_n \approx E/10$.

Let us now consider the stress concentration produced by cracks. The stress field around a crack tip can be determined by linear elastic fracture mechanics. Common solutions can be found in standard text books. [51, 53]. A material is treated as a linear elastic continuum and a crack is assumed to be a "mathematical" section through it (having a crack root radius of zero). Under plane strain conditions the components of the local stress field on a volume element, σ_{ij}, in a region near the crack tip is space depend and can be expressed as (polar coordinates r and θ; origin at the crack tip) [51, 53]:

$$\sigma_{ij}(r,\theta) = (K/\sqrt{2\pi r}) \cdot f_{ij}(\theta) \quad . \tag{2}$$

The tensor f_{ij} is a function of the angle θ and has values between zero and one. The function can be found in text books [51, 53]. The stress field scales with the stress intensity factor K, given by

$$K = \sigma Y \sqrt{\pi a} \quad , \tag{3}$$

where σ is the nominal stress in the un-cracked body, a is the crack length and Y is a geometric correction factor (for not uniaxial tensile loadings, Y may also depend on the loading situation). Data for the geometric factor can also be found in literature [54-56]. For cracks, which are small compared to the component size (this is the general case in ceramics), Y is of the order of unity. Important examples of idealised crack

geometry are "penny shaped" cracks in the volume of a body and straight-through edge cracks. The geometric correction factor is $Y = 2/\pi$ for small cracks and in the latter case it is $Y = 1.12$.

The components of the stress tensor σ_{ij} have a square root singularity at the crack tip. They therefore become infinite at the tip of a crack and inevitably exceed the theoretical strength, even at very weak loads or small crack sizes. Note that this corresponds to the solution for an elliptical hole with a tip radius of zero (eq. 1b). There exist cracks under load which do not grow. Consequently, an additional condition for the growth of cracks must exist, and this was found by Griffith who analysed the energy changes associated with the extension of a single crack in a brittle material [57].

According to Griffith, crack growth only occurs, if the crack extension reduces the total energy in a body. There exists a "critical" crack length a_c: cracks of larger or equal size extend, but smaller cracks are stable. Griffith analysis shows that the fracture stress (the strength) is related to the critical crack length according to the relationship $\sigma_f \propto a_c^{-1/2}$.

In the framework of linear elastic fracture mechanics, the total energy released by crack growth (work done and elastic energy released) under plane strain conditions is given by the product of the strain energy release rate [51, 53]

$$G = \frac{K^2}{E} \quad .$$

(4)

and the newly cracked area ($t \cdot \delta a$). Fracture occurs if the released energy (per newly cracked area) reaches or exceeds the energy necessary to create the new crack:

$$G \geq G_c \quad .$$

(5)

Inserting eq. 4 in eq. 5 gives the so called Griffith/Irwin fracture criterion

$$K \geq K_c \quad .$$

(6)

The critical stress intensity factor K_c is called fracture toughness. It is defined by

$$K_c = \sqrt{E \cdot G_c} \quad .$$

(7)

A theoretical lower bound for the fracture energy is the energy of the new surfaces (2γ). In reality the fracture energy is at least one order of magnitude higher, because energy dissipating processes ahead of the crack tip (in process zones, [58]) or behind the crack tip (at crack bridges, [59-61]) occur. A typical value for the surface energy of ceramics is in the order of 1 J/m^2 and values for fracture energy range between 10-3000 J/m^2.

4.2. Tensile Strength of Ceramic Components and Critical Crack Size

The tensile strength of a component can be determined by inserting eq. 3 in eq. 6 and solving for the stress (at the moment of fracture):

$$\sigma_f = \frac{K_c}{Y\sqrt{\pi a_c}} \quad . \tag{8}$$

The strength scales with the fracture toughness and is inversely proportional to the square root of the critical crack size a_c. This corresponds to the former results of the Griffith analysis.

Strength test results on ceramic specimens show, in general, large scatter. This follows from the fact, that in each individual specimen the size of the critical crack is a little different. Rearranging eq. 8 gives a relationship for the critical crack size (Griffith crack size) in a specimen:

$$a_c = \frac{1}{\pi} \cdot \left(\frac{K_c}{Y\sigma_f}\right)^2 \quad . \tag{9}$$

Figure 7 shows several fracture origins in ceramic materials. It is obvious that there exists a strong correlation between the occurrence of dangerous flaws and the processing of a material. Typical volume flaws, which may act as fracture origins, are agglomerates of second phase, large pores, inclusions, large grains or agglomerations of small pores [17, 19]. Typical fracture origins at the surface are grinding scratches and contact damage. Even grooves at grain boundaries may act as fracture origins [62].

For many ceramic materials the ratio K_c / σ_f is of the order 1/100 √m. If fracture starts in the interior of the component the geometric correction factor for a penny shaped crack ($Y = 2/\pi$) can be used to calculate the corresponding Griffith crack size, giving a typical $a_c \approx 80$ μm. The size of critical flaws reflects the state of the art in minimizing microstructural defects during the processing of ceramic specimens and components.

In **Figure 7** it can be recognised that the Griffith crack size is often a little larger than the size of the critical flaw. Several reasons can be identified for that behaviour. Some of them will be discussed in the following.

In most materials the resistance to crack propagation is not constant. It increases at the start of crack extension and reaches, after some crack growth, a plateau value [3, 4]. In consequence, the toughness may depend on the testing conditions [4]. Under the conditions of typical fracture toughness tests the toughness may be a little higher than under strength testing conditions. Thus in the evaluation of the Griffith crack size, a too high value for toughness is sometimes used, leading to overestimation.

In most strength tests some SCCG happens before final fracture occurs. This means that the cracks start to grow at stress intensity factors smaller than the fracture toughness. The Griffith crack size then corresponds to the size of the flaw plus the crack extension due to SCCG.

Finally it should also be remembered that flaws are not truly cracks and that a materials' microstructure is not an ideal continuum, i.e. flaws and cracks have different stress fields. Flaws cause a (finite) stress concentration (see eq. 1), but cracks cause a stress singularity at their tips (see eq. 2). As discussed earlier for elliptical holes, a major semi-axis to tip radius ratio of several thousand would be necessary to produce the stress concentration to break the bonds at the tip. At first glance this seems not to be probable, but it is not completely unreasonable. Very sharp edges may occur on processing defects. An example is shown in **Figure 7b**. The fracture origin is a large pore, which, on a meso scale, can be modelled by a spherical hole with a radius of about 25μm. But many sharp grooves at the grain boundaries can be detected. These could be described as sharp notches distributed around the sphere [63, 64]. It is obvious that the tip radius of these grooves in front of the pore is much less than 1 μm, giving a high aspect ratio.

In summary fracture of brittle materials is a complex topic. The fracture process is largely influenced by the local microstructure, which makes the aspects of a suitable statistics significant. These aspects will be tackled in section 5.

(a)

(b)

(c)
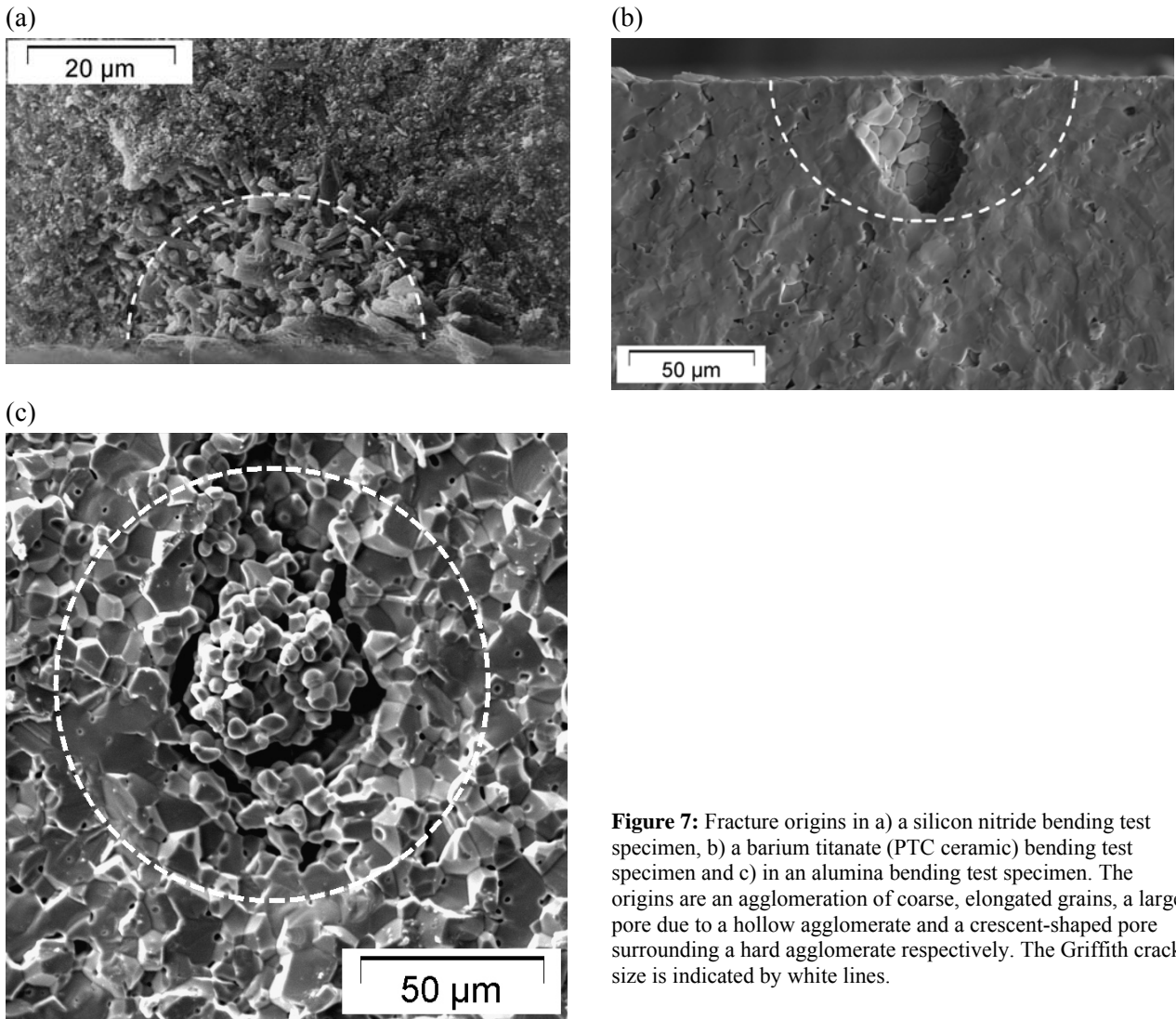
Figure 7: Fracture origins in a) a silicon nitride bending test specimen, b) a barium titanate (PTC ceramic) bending test specimen and c) in an alumina bending test specimen. The origins are an agglomeration of coarse, elongated grains, a large pore due to a hollow agglomerate and a crescent-shaped pore surrounding a hard agglomerate respectively. The Griffith crack size is indicated by white lines.

5. Probabilistic Aspects of Brittle Fracture

In series of fracture experiments on ceramic specimens two important observations can be made: the probability of failure increases with the load amplitude and with the size of the specimens [2-4, 14]. This strength-size effect is the most prominent and relevant consequence of the statistical behaviour of strength of brittle materials. These observations cannot be explained in a deterministic way using the simple model of a single crack in an elastic body. Their interpretation requires the understanding of the behaviour of many cracks distributed throughout a material.

In the following it is assumed that many flaws, which behave like cracks, are stochastically distributed in a material. For convenience, it is assumed at first that the stress state is uniaxial and homogenous and that cracks are perpendicularly oriented to the stress axis. More general situations will be discussed later.

It is further assumed that cracks do not interact (this means that their separation is large enough for their stress fields not to overlap). This assumption is essential for the following arguments and is equivalent to the weakest link hypothesis: this failure of a specimen is triggered by the weakest volume element or, in other words, by the largest flaw it contains.

5.1. Fracture Statistics and Weibull Statistics

Using the assumptions made above, a cumulative probability of fracture (the probability that fracture occurs at a stress equal to or lower than σ) can be defined [65]:

$$F_S(\sigma) = 1 - \exp\left(- N_{c,S}(\sigma)\right)$$

(10)

$N_{c,S}(\sigma)$ is the mean number of critical cracks in a large set of specimens (i.e. the value of expectation). The symbol S designates the size and shape of a specimen. The number $N_{c,S}(\sigma)$ depends on the applied load via a fracture criterion, e.g. eq. 5 or eq. 6. At low loads, the number of critical cracks is small: $N_{c,S}(\sigma) \ll 1$. This is typical for the application of advanced ceramic components, since they are designed to have a high reliability. In this case the probability of fracture becomes equal to the number of critical cracks per specimen: $F_S(\sigma) \approx N_{c,S}(\sigma) \ll 1$. At high loads this number may become high: $N_{c,S}(\sigma) \gg 1$. Then some of the specimens may contain even more critical cracks than the mean value $N_{c,S}$. Nevertheless, the (small) probability still exists that, in some individual specimens, no critical crack occurs. Therefore, there is always a non-vanishing probability of survival for an individual specimen and the probability of fracture only asymptotically approaches one for very high values of $N_{c,S}(\sigma)$ (eq. 10).

It should be noted that the fracture statistics given in eq. 10 describe the experimental observations mentioned at the beginning of this chapter correctly: the probability of failure increases with load amplitude (because at higher loads more cracks become critical); and the mean strength decreases with specimen volume (since the probability of finding large cracks in large specimens is higher than in small specimens). Of course, at a given load, a specimen can either fail or survive. Therefore, it holds: $R_S(\sigma) + F_S(\sigma) = 1$, with $R_S(\sigma)$, the reliability, being the probability of a specimen with size S surviving the stress σ.

To establish analytically the dependence of the probability of failure on the applied load, more information on the crack population involved is needed [66-70]. If a homogeneous crack-size frequency density function $g(a)$ exists, the mean number of critical cracks per unit volume is

$$n_c(\sigma) = \int_{a_c(\sigma)}^{\infty} g(a) \, d a \quad ,$$

(11)

and the mean number of critical cracks (Griffith cracks) per specimen is $N_{c,S}(\sigma) = V \cdot n_c(\sigma)$, with V being the volume of the specimen. (For an inhomogeneous crack size distribution the number of critical flaws per specimen results from integration of the local critical crack density $n_c(\sigma, \vec{r})$ over the volume, with $\vec{r}$ being the position vector.) The strength-size effect is a consequence of this relationship.

The stress dependency of the critical crack density results from the stress dependence of the Griffith crack size, which is the lower integration limit in eq. 11.

In most materials the size frequency density decreases with increasing crack size. i.e. $g \propto a^{-p}$, with p being a material constant. For such cases eq. 11 can easily be integrated [67, 70, 71]. Inserting the result in eq. 10 gives the well-known relationship for Weibull statistics [72, 73]:

$$F(\sigma,V)=1-\exp\left[-\frac{V}{V_0}\left(\frac{\sigma}{\sigma_0}\right)^m\right] \quad . \tag{12}$$

The Weibull modulus m describes the scatter of the strength data. The characteristic strength σ_0 is the stress at which, for specimens of volume $V = V_0$, the failure probability is: $F(\sigma_0,V_0)=1-\exp(-1)\approx 63\,\%$.

Independent material parameters in eq. 12 are m and $V_0\sigma_0{}^m$; the choice of the reference volume V_0 influences the value of the characteristic strength σ_0.

The material parameters in the Weibull distribution are related to the fracture toughness of the material and to parameters from the size frequency density of the cracks. Details can be found in [62]. For example, as shown in the noteworthy paper of Jayatilaka et al. [67], the Weibull modulus only depends on the slope of the crack size frequency distribution: $m = 2 \cdot (p-1)$.

The derivation indicated above clearly shows that the Weibull distribution is a special case out of a class of more general crack-size frequency distributions [65, 69, 70]. Especially the type of flaw distribution may have influence on the strength distribution function. This point will be discussed later. This notwithstanding, almost all sets of strength data determined on ceramics reported so far can be fitted nicely by a Weibull distribution function. Therefore, the Weibull distribution is widely used to describe strength data and for designing with brittle materials. Typically, advanced ceramics have a Weibull modulus between 10 and 20, or even higher. For classical ceramics the modulus is between 5 and 10.

The following sections 5.1.1 to 5.1.3 deal with the Weibull distribution for several special situations and may be skipped by a reader who does not want to go into such details.

5.1.1. Weibull Distribution for Arbitrarily Oriented Cracks in a Homogeneous Uniaxial Stress Field

In general the orientation of cracks will depend on the processing conditions of specimens or components. Furthermore, their distribution may be random or there may be some preferred orientation. Up to now, it has been assumed that cracks are perpendicularly oriented to a uniaxial tensile stress field. In fact, this assumption is, in general, not necessary and has only been made to make the above arguments simple.
Let us first discuss the influence of random crack orientation in a homogeneous uniaxial tensile stress field. The most dangerous cracks are those oriented perpendicularly to the direction of stress. In this case, the crack boundaries are pulled apart by the applied stress (uniaxial tensile loading, opening, mode I). If cracks are parallel to the uniaxial stress direction, the crack borders are not opened by the stresses and they do not disturb the stress field. Clearly, this type of loading is harmless. For any crack orientation between these extremes, some in-plane (sliding) or out-of-plane (tearing) shear loading (mode II and mode III) of the cracks occurs. Then, the strain energy release rate is $G = K_I{}^2/E' + K_{II}{}^2/E' + K_{III}{}^2(1-\mu)/E$, where K_I, K_{II} and K_{III} are the stress intensity factors for each mode of loading and $E' = E$ for plane stress and $E' = E/(1-\mu^2)$ for plane strain conditions [51]. μ is the Poisson ratio.

To describe the action of many cracks in a uniaxial stress field, not only the crack-size distribution, but also the distribution of crack orientations should be known. Such analysis shows that the results of the last chapter remain valid, but the characteristic strength σ_0 is influenced by the fact that, in the general case, the number of critical cracks not only depends on the length but also on the orientation of the crack [67].

5.1.2. Weibull Distribution for Arbitrarily Oriented Cracks in an Inhomogeneous Uniaxial Stress Field

For inhomogeneous but uniaxial stress fields a generalisation of eq. 12 can be made - see Weibull [72, 73]:

$$F\left(\sigma_r, V_{eff}\right) = 1 - \exp\left[-\frac{V_{eff}}{V_0}\left(\frac{\sigma_r}{\sigma_0}\right)^m \right] \quad . \tag{13}$$

Where V_{eff} the effective volume of a component is given by the integration of the stress field over the volume:

$$V_{eff} = \int_{\sigma > 0}\left(\frac{\sigma(\vec{r})}{\sigma_r}\right)^m dV \quad , \tag{14}$$

where σ_r is an arbitrary reference stress. The integration is done only over volume elements where the stress $\sigma(\vec{r})$ is tensile. Any damaging action of compressive stresses is, therefore, neglected. However, since the compressive strength is generally around one order of magnitude higher than the tensile strength, this is, in fact, quite reasonable for any case where the compressive stress amplitude is not more than about three times larger than the tensile stress amplitude.

Usually, the effective volume is defined to be the volume of a tensile test specimen which would yield the same reliability as the component if loaded with the reference stress. (Remark: Other definitions are also possible. For example STAU uses the most damaging stress state (i.e. the isostatic (tri-axial)) stress state for the definition of the equivalent stress [74]).

The effective volume is related to the reference stress via the equation: $\sigma_r{}^m V_{eff} = \sigma_0{}^m V_0$. In general the maximum in the stress field is used as the reference stress (for example: in bending tests the outer fibre stress is commonly used). Since, for advanced ceramics, the Weibull modulus is a relatively high number (e.g. $m = $ 10-30), only the most highly loaded volume elements (stress more than 80 % of the maximum) contribute significantly to the effective volume and so the effective volume approximates to the "volume under high load". It should be noted that, if a stress lower than the maximum tensile stress is selected as the reference stress, then the effective volume may become large – possibly larger even than the real size of the component.

For simple cases, e.g. the stress field in a bending specimen, the calculation of the integral in eq. 14 can be made analytically, but in general, and especially in the case of components, a numerical solution is necessary. For each loading case the calculations has to be done only once, because the integral scales with the load amplitude. As mentioned before, for modern ceramic materials the Weibull modulus can be high. Then, the numerical determination of the effective volume may become difficult, especially if high stress gradients exist. Commercial tools which can post process data generated in an FE stress analyses are available. Examples are STAU [74] or CARES [75], effective volumes for standardized flexure bars and cylindrical rods in flexure have been published [76, 77]

5.1.3. Weibull Distribution in a Poly-axial Stress Field

Poly-axial stress states can be taken into account by replacing the stress σ in the above considerations by an equivalent stress σ_e:

$$\sigma \to \sigma_e \quad . \tag{15}$$

The equivalent (uniaxial) stress is the uniaxial tensile stress which would have the same damaging action as an applied poly-axial stress state. The proper definition of the equivalent stress depends on the type of the fracture causing flaws and how such flaws act as cracks – note, this is still a matter of some debate. The definition also depends on the fracture criterion for poly-axial stress states, and this should also take the action of compressive stresses into account. Precise information on real flaw distributions and multi-axial strength data are rarely available and the large scatter of strength values makes unambiguous interpretation of data difficult.

Many different proposals for the definition of the equivalent stress in ceramics can be found in the literature [3, 4, 78-81], but a consensus on the best choice still does not exist. For small data sets, of the kind most commonly tested, scatter obscures the differences between reasonable alternative fracture criteria. The most frequently used criteria are described below.

The first principle stress criterion (FPS) simply assumes that only the first principle stress σ_I has to be taken into account:

FPS criterion [3, 4]: $\qquad \sigma_e = \sigma_I \qquad$ for $\sigma_I > 0$

$\qquad$ and $\qquad \sigma_e = 0 \qquad$ for $\sigma_I \le 0$. $\qquad$ (16a)

The principle of independent action (PIA) accounts for the action of all principle stresses (σ_I, σ_{II} and σ_{III}) independently:

PIA criterion [78]: $\qquad \sigma_e = (\sigma_I{}^m + \sigma_{II}{}^m + \sigma_{III}{}^m)^{1/m} \quad$ for $\sigma_I > 0$

$\qquad$ and $\qquad \sigma_e = 0 \qquad\qquad\qquad$ for $\sigma_I \le 0$. (16b)

The action of compressive stresses is neglected in both cases.

It is expected that the FPS criterion applies nicely for flat, crack-like flaws. For more spherical flaws, which have similar stress concentrations in all directions, the PIA criterion seems to be more appropriate [63]. It should noted, however, that the influence of the criterion on the equivalent stress is relatively limited: for a material with a Weibull modulus of $m = 20$ and in a biaxial stress state, the FPS equivalent stress is $\sigma_{e,FPS} = \sigma_I$ whereas the PIA equivalent stress is $\sigma_{e,PIA} = 2^{1/m}\sigma_I \approx 1.04\,\sigma_I$, i.e. the difference is only four percent. This small difference between the equivalent stresses is often hidden by the scatter of data. To give an example, if the Weibull parameters are determined on a sample of 30 specimens and for $m = 20$, the 90 % confidence interval of the characteristic strength ranges from 98 % to 102 %, and that of the Weibull modulus from 79 % to 139 %. Therefore, a clear selection between the different criteria can hardly be done. Of course, the equivalent stress should also be used for the proper definition of the effective volume. This possibility (for several different definitions of the equivalent stress) is also accounted for in commercial FE programs [74, 75].

5.2. Application of the Weibull Distribution: Design Stress and Influence of Specimen Size

Up to now the Weibull distribution function and the ideas sketched above form the basis of the state of the art mechanical design process for ceramic components [2-4]. Consequently, the strength testing [82-84] of ceramics and the determination of Weibull distributions is standardised [6, 85-87].

In this section, examples of strength statistics and the resulting size effect are given. Used are data determined in a European research program organised by ESIS, which conceived to determine a complete set of design relevant data for a commercial silicon nitride ceramics. Details on the ESIS reference material testing program can be found in [13, 88, 89].

An example for a strength distribution is shown in **Figure 8**, which shows the cumulative probability of failure versus 4-point bending strength data. The sample consisted of 42 individual experiments and is larger than in most other reported cases. The logarithmic scales have been chosen in such a way that the Weibull distribution is represented by a straight line. The distribution fits nicely to the measured data. The reference stress used is the maximum surface bending stress and the normalising volume used is $V_{eff} = V_0 = 7.7$ mm^3.

The Weibull modulus is $m = 15.5 \pm 3$ and the characteristic strength of the sample resulting from the sampling procedure is $\sigma_0 = 844 \pm 15$ MPa. The indicated scatter relates to the 90 % confidence intervals. The distribution function can be used to determine the relationship between reliability and the necessary equivalent design stress $\sigma_{e,r,R}(V_{eff})$. For a component with the effective volume V_{eff} it holds:

$$\sigma_{e,r,R}(V_{eff}) = \sqrt[m]{\frac{V_0 \sigma_0{}^m}{V_{eff}} \cdot \ln\frac{1}{R}} \quad . \tag{17}$$

To give an example, for $V_{eff} = V_0$, let us determine the maximum allowable stress for a reliability of $R = 99.9999$ % in the bending tests shown in **Figure 8.** Following eq. 17 the stress is $\sigma_{e,r,R}(V_{eff}) = \sigma_0 \cdot (\ln 1/R)^{1/m}$. Inserting the numerical values for R, σ_0 and m gives $\sigma_{e,r,0.999999}(V_0) = 0.41 \cdot \sigma_0 = 348$ MPa. In other words, it is expected that one specimen out of a million would fail at a stress equal to or smaller than 348 MPa. This stress is also indicated in **Figure 8**. Remember, the characteristic strength of the data set is 844 MPa.

It should be noted that, for the selected example, the design stress determined by probabilistic means corresponds - in a deterministic design approach - to a "safety factor" of about 844 MPa / 348 MPa = 2.4. The advantage in the probabilistic approach is that a realistic reliability can be determined and that total safety, which does not exist in reality, is not implied.
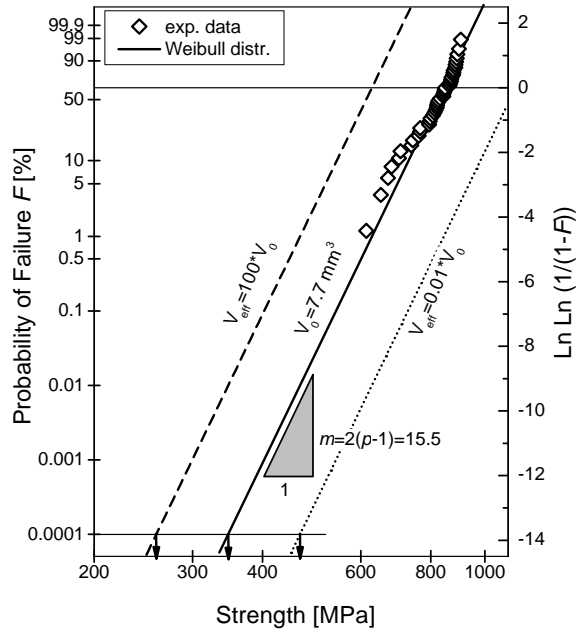
Figure 8: Bending strength test results for a silicon nitride ceramic. Plotted is the probability of failure versus the strength. The straight lines represent Weibull distributions. The measured Weibull distribution has a modulus of $m = 15.5$ and the characteristic strength is 844 MPa. Also shown are Weibull distributions for specimens with a 100 times larger (left) and a 100 times smaller (right) effective volume. Indicated are the 10^{-4} % failure probabilities and the design stresses for each set of specimens respectively.

Now let us discuss the influence of the volume under load. For two sets of specimens of different volume (indicated by the indices 1 and 2) the (equivalent) stresses to achieve the same reliability R must follow the condition:

$$\sigma_1(R)^m V_1 = \sigma_2(R)^m V_2 \quad \text{or} \quad \sigma_2(R) = \sigma_1(R) \cdot \left(\frac{V_1}{V_2}\right)^{1/m} \quad , \quad (18)$$

where $\sigma_1(R)$ and $\sigma_2(R)$ are the corresponding equivalent reference stresses to get the desired reliability R and V_1 and V_2 are the corresponding effective volumes of the specimens. If, in the above example, the effective volume is increased 100 times, the design stress decreases by a factor of $100^{1/15.5} = 0.72$ and becomes $0.72 \cdot 348$ MPa $= 234$ MPa (for a 100 times smaller volume it becomes 451 MPa). These estimates assume a single flaw type population initiating failure in all specimen sizes.

The Weibull distributions functions for the large and the small specimens are also shown in **Figure 8.** It can be recognised that the Weibull line is shifted to lower strength values in the first case and to higher strength values in the latter case.

The dependence of strength on the specimen size is the most significant effect caused by its probabilistic nature. As discussed above it may have a dramatic influence on the design stress. To demonstrate that influence, **Figure 9** again shows experimental results from the ESIS reference materials testing program. Results of three point and four point bending tests (uniaxial stress fields) and of ball-on-three balls tests (biaxial stress field) are reported (for details of the testing procedures see [88-92]). The PIA criterion was used to calculate the equivalent stress. The effective volume of the specimens is in a range between about 10^{-3} and 10^2 mm^3. In this range the data follow the trend determined by the Weibull theory. The dashed lines describe the limits of the 90 % confidence interval for a data prediction based on the 4-point bending data presented in **Figure 8**. The characteristic strength of the individual samples varies from about 800 MPa (for the largest specimens) up to almost 1200 MPa (for the smallest specimens).

Of course measurement uncertainties should also be considered in proper design. This point will be discussed in section 5.3.
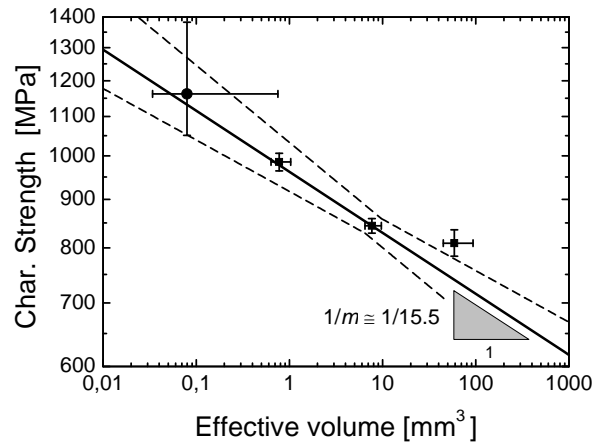
Figure 9: Strength test results of a silicon nitride ceramic. Shown are data from uniaxial and biaxial strength tests. To determine the equivalent stress the PIA criterion was used. Plotted in log-log scale is the characteristic strength of sets of specimens versus their effective volume. The solid line indicates the trend predicted by the Weibull theory. Scatter bars and the dashed lines refer to the 90 % confidence intervals due to the sampling procedure (see section 0). The relatively large scatter of the sample with the smallest specimens results from the small number of tested specimens.

5.3. Experimental and Sampling Uncertainties, the Inherent Scatter of Strength Data and Can a Weibull Distribution be Distinguished from a Gaussian distribution?

In most cases strength data of ceramics are determined in bending tests following EN 843-1 [82], ASTM 1161 [83], ISO 14704 [6] or JIS R 1601 [84]. The measurement uncertainty of an individual strength measurement should be less than 1 % [93, 94]. The determination of the Weibull distribution is standardised in EN 843-5 [85]. Following this standard (and other similar American [86] and Japanese [87] standards) the Weibull distribution function has to be measured on a sample of "at least" 30 specimens (due to high machining costs, it is not common practice to test larger samples).

The failure probability of an individual strength test is unknown, but it can be estimated with an estimation function. Many proposals exist for appropriate estimation functions, but the difference between these functions is – from practical point of view – not very relevant: for large sample sizes the differences are very small and for small sample sizes the scatter of data is larger than the difference between the different estimation functions. In standards, e.g. in EN 843-5 [85], the function

$$F_i = \frac{2i-1}{2N} \tag{19}$$

is used. F_i is the estimated failure probability of the ith specimen (the specimens are ranked with increasing strength). The number of specimens in the sample is N (sample size). The range of failure probabilities which can be determined increases with sample size (from $F_1 = 1/2N$ to $F_N = (2N-1)/2N$. For a sample with $N = 30$ the range goes from $F_1 = 1/60$ to $F_{30} = 59/60$.

The inherent scatter of the Weibull parameters can be determined using Monte Carlo simulation techniques. Let us generate (by "throwing dice") a random number between zero and one. This random number is defined to be the failure probability of a specimen. Then, for a material with a known Weibull distribution, the corresponding strength value can be generated using eq. 12. By repeating this procedure N times a virtual sample of size N is determined. In this way millions of samples can be generated with limited effort. This technique can be used to study the difference between sample and population [70].

It is obvious that the difference between sample and population may become larger the smaller a sample is. The minimum sample size of $N = 30$ specified in standards is a compromise between the large cost of specimen preparation and accuracy. Nevertheless, it should be noted that for $N = 30$ the uncertainty is still relatively large. **Figure 10** shows the confidence intervals which result from the sampling procedure, for the Weibull modulus and the function $\sigma_0^{\ m}$ (the scatter of the characteristic strength depends on the modulus) in dependence of the sample size respectively. Of course in most practical situations the "sampling" is hypothetical, so these values represent the uncertainty should the experiment be repeated.

(a)   (b)
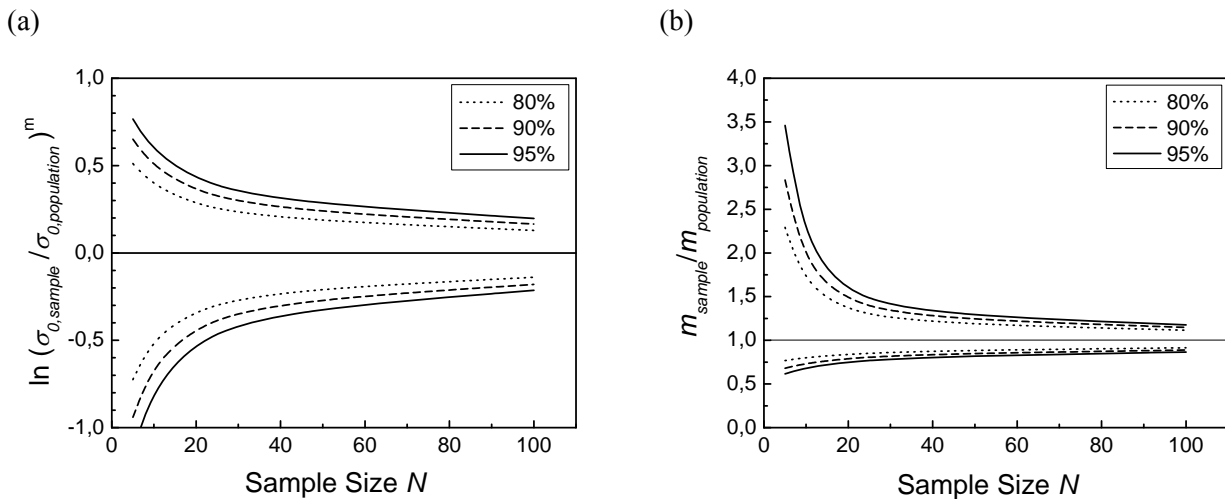
Figure 10: Confidence intervals in dependence of sample size a) for the Weibull modulus and b) for $\sigma_0^{\ m}$. The confidence intervals for the characteristic strength depend on the modulus.

It is important to realise that on the basis of experiments it is almost impossible to differentiate whether a population has a Weibull distribution or another type or distribution. In **Figure 11** the data and the Weibull distribution of **Figure 8** are plotted in a linear and in a log-log scale. Also shown is a Gaussian (Normal) distribution function, which fits to the experimental data.
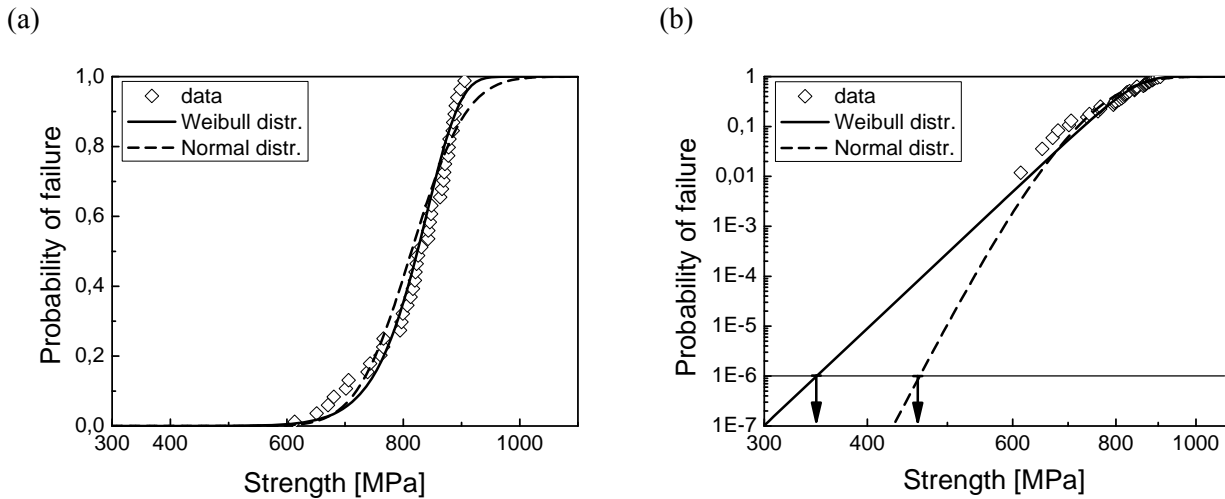
Figure 11: Strength distribution of a silicon nitride ceramic (same data as in **Figure 8**). A Weibull distribution function (full curve) and a Gaussian distribution function (dashed curve) are fitted to the data. The data are plotted a) in a linear and b) in a log-log scale. Although both distributions fit the experimental data very well, the extrapolation to low probabilities of failure leads to quite different results.

Both functions describe the experimentally determined part of the distribution very well, but they show big differences at low failure probabilities, where no experimental data exist (see eq. 10). This range of low probabilities, however, is exactly the range where distribution curves are applied to predict the reliability of components. The $R =$ 99.9999 % design stress determined by Weibull analysis is 348 MPa and determined on the basis of the Gaussian function it is 460 MPa, i.e. it is more than 30 % larger! This large difference demonstrates the need for proper selection of the distribution function - but this can hardly be done on the basis of a small sample. From eq. 19 and **Figure 11** it can be seen that several 1000 strength tests would be needed to experimentally detect a difference between a Weibull and a Gaussian distribution curve [62, 95]. This effort exceeds the possibilities of any research laboratory. But the theoretical arguments given at the beginning of section 5 tell us that a Weibull distribution is more appropriate to describe the strength data of brittle materials than a Gaussian distribution. Weibull statistics also implies a size effect on strength (the Gaussian distributions does not), and such an effect has been demonstrated empirically (see **Figure 10**). It can therefore be stated that the strength of this material is Weibull distributed.

5.4. Influence of Microstructure: Flaw Populations on Fracture Statistics

It follows from eq. 10 that the strength distribution is strongly related to the flaw distribution. In the preceding paragraphs it has been shown that the Weibull distribution occurs for volume flaws with a size distribution which follows an inverse power law: $g \propto a^{-p}$. It should be realised that the Weibull distribution is a direct function of the flaw-size distribution (see eqs. 10 and 11). Following this logic, any strength measurement can be interpreted as a measurement of the relative frequency distribution function of flaw sizes (albeit smeared by the scatter of data as discussed above **Figure 12** shows the relative frequency of flaw sizes determined on the basis of the strength data shown in **Figure 8**. The frequency distribution follows the inverse power law (note the wide range of frequencies determined with this set of data) and the strength distribution is a Weibull distribution for that reason. A material with that behaviour is called a Weibull material.

Other types of flaw distributions can also occur. Examples are bi- and multimodal flaw populations [69, 70, 96], the simultaneous occurrence of volume and surface defects [65, 70], or the occurrence of narrow peaked flaw populations [70, 71]. To take the influence of several concurrently occurring flaw distributions into account their mean number per specimen (see eq. 12 and [65]) can simply be superposed:

$$N_{c,S}(\sigma) = \sum_i N_{c,S,i}(\sigma) \quad . \tag{20}$$

$N_{c,S,i}(\sigma)$ is the mean number of critical defects of population i per specimen. The size S of the specimen can – depending of the type of flaw and the stress field in the specimen – relate to the (effective) volume (for volume flaws), the (effective) surface (for surface flaws) or the (effective) edge length (for edge flaws, [70]). Multimodal flaw distributions cause perturbing structures in the strength distribution curves (bends or peaks in the straight "Weibull"-line as shown in **Figure 13**), which cause a deviation from the simple analytic form of the Weibull distribution given in eq. 12.
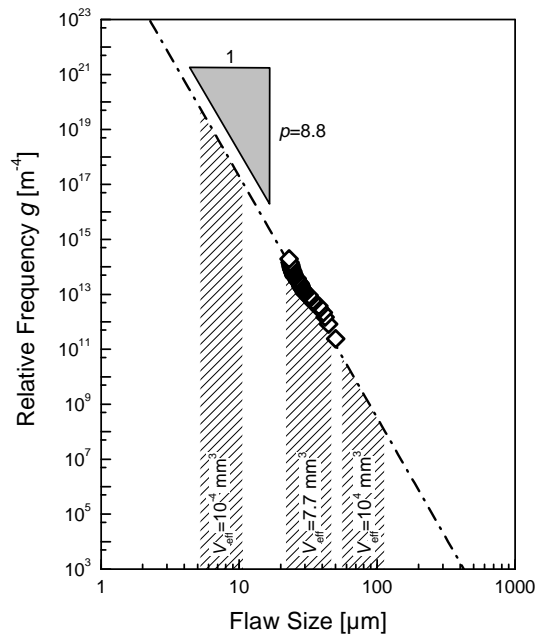
Figure 12: Relative frequency of flaw sizes versus their size. The distribution is plotted in a log-log scale. Shown are data of the same experiments as in **Figure 8**. The data are nicely arranged around a straight line, which indicates the Weibull behaviour of the material (for details of the data evaluation see [62]). The grey underlined areas correspond to the parameter ranges accessible with a sample of size 30 for specimens having the volume of the bending specimens (middle), a much larger volume (right) and a much smaller volume (left). It can be recognised that the size of fracture origins of specimens of different volumes is expected to be found in different ranges.

Figure 13 shows the example of a bi-modal distribution. A narrow peaked distribution is superimposed on to a wide flaw-size distribution. Graph a) shows the relative frequency distribution of flaw sizes (top) and the density of critical flaws (below). The corresponding probabilities of failure are shown as a dashed line in Graph b). Also shown are results of Monte Carlo simulations. The open symbols refer to a sample which represents the population very well, and the solid symbols refer to a sample which seems to behave like a Weibull distribution. A few percent of all samples (size 30) have that behaviour (it should be noted that this simulation exactly reflects the sampling procedure). Figure c) shows the size effect of strength. Due to the relatively small scatter of the characteristic strength data (see 90 % confidence intervals for samples of size

30) an investigation of the size effect on strengths seems to be an appropriate way to determine the fracture statistics of a material.

In summary, it has to be stated that the strength distribution is a direct function of the size distribution of the flaws which act as fracture origins. The analytical Weibull equation (eq. 12) is a special case of a more general distribution which often, but not always, occurs in brittle materials. Therefore, extrapolations out of the experimentally explored parameter area should be considered with care. Bimodal and multi-modal flaw populations cause perturbations in the strength distribution and can cause large deviations from the behaviour expected from a Weibull material. It should, however, also be recognised that on the basis of fitting distributions to the results of strength tests, the true type of the distribution can hardly be determined, because the data sets are too small to describe the tail ends of the distribution curve. The best way to determine distribution curves in a wide range is the testing of several subsets of specimens of different specimen size [62, 71, 97].

5.5. Limits for the Application of Weibull Statistics in Brittle Materials

There are some prerequisites for the occurrence of a Weibull distribution [65, 67, 71]. The most important are: i) the structure fails if one single flaw becomes critical (weakest link hypothesis) and ii) dangerous flaws do not interact.

These prerequisites are not valid for ductile materials and in fibre reinforced materials. In the first case, stresses are accommodated by plastic deformation and in the latter case, load can be transferred from the matrix into the fibres. Furthermore, negligible interaction between flaws is only possible if the flaw density is low. Weibull theory, therefore, does not apply for porous materials.

It has also been shown that Weibull theory also does not apply for very small specimens [62]. In such specimens the fracture causing flaws are also very small. For a Weibull material (i.e. for a material with relative flaw density corresponding to $g \propto a^{-p}$) the density of the flaws becomes so high for small flaws that interaction between the flaws will occur.

In cases where the relative frequency of flaw sizes has a shape different to that of a Weibull material, the Weibull modulus becomes stress dependent. The same happens for bi- and multi- modal flaw distributions [70, 71].

There are many other reasons for deviations from Weibull behaviour (eq. 12), e.g. internal stress fields [70], gradients in the mechanical properties [69], or if the toughness of the material increases with the crack extension (R-curve behaviour) [71]. In these cases too, the modulus and the characteristic strength become stress and volume dependent, respectively.

In short, it can be stated that the Weibull distribution is often, but not always, the appropriate strength distribution function. Extrapolations have, therefore, to be handled with care. It is helpful in many cases to determine strength data on specimens of different volume, since this procedure enlarges the parameter ranges on which extrapolation is based. Fractography is useful for ascertaining if a flaw distribution is mono- or multi-modal.

(a)

(b)

(c)
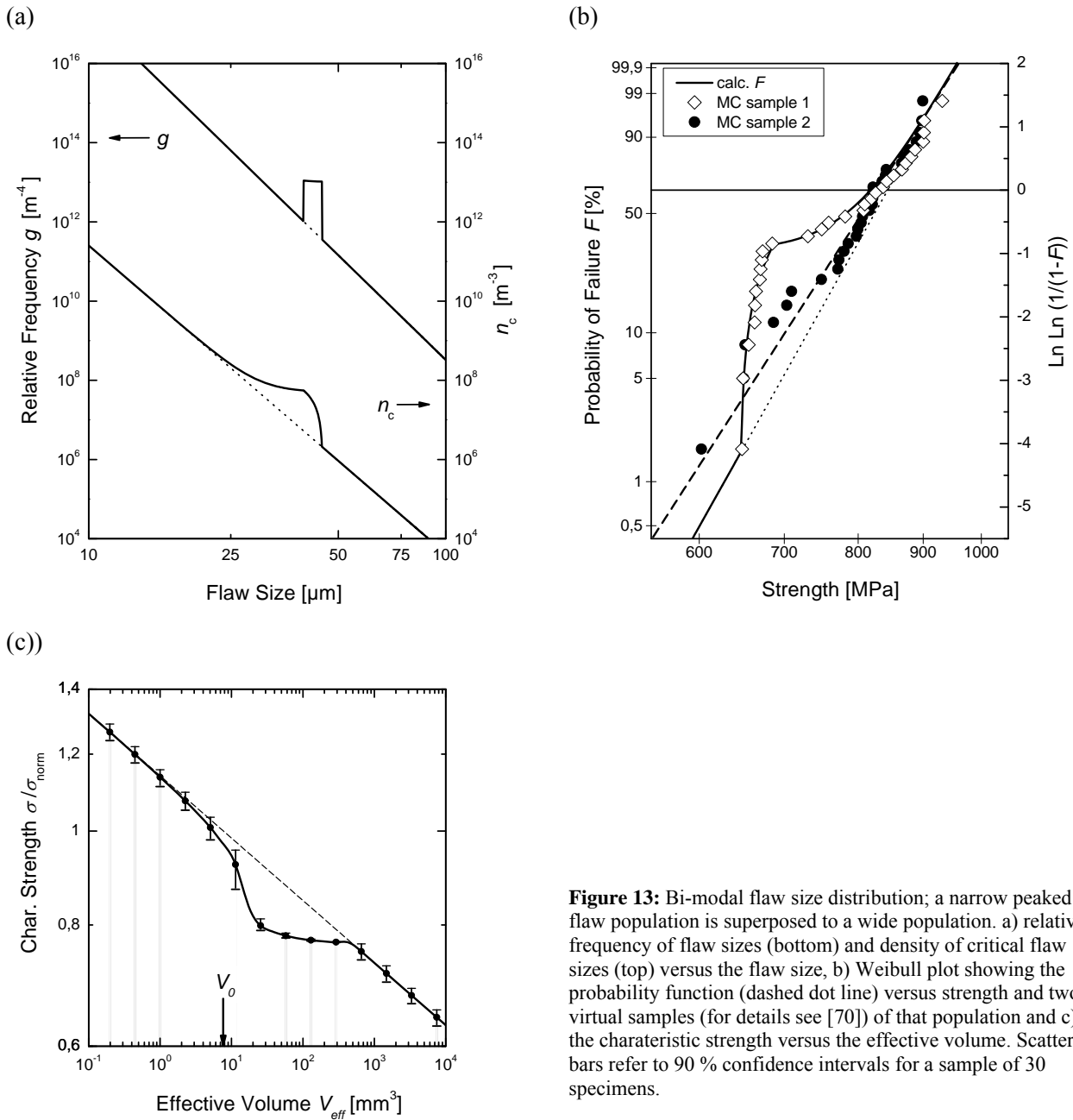
Figure 13: Bi-modal flaw size distribution; a narrow peaked flaw population is superposed to a wide population. a) relative frequency of flaw sizes (bottom) and density of critical flaw sizes (top) versus the flaw size, b) Weibull plot showing the probability function (dashed dot line) versus strength and two virtual samples (for details see [70]) of that population and c) the charateristic strength versus the effective volume. Scatter bars refer to 90 % confidence intervals for a sample of 30 specimens.

6. Delayed Fracture

In the last section we focused on fast, brittle fracture, in which a specimen under the action of a given load either fails immediately after the application of the load or does not fail at all. But it is well-known that components also fail after some time in service. Of course, under a varying load, this may happen due to the incidental occurrence of an extra high peak in the load spectrum. But delayed fracture may also be related to types of defects, which slowly grow to a critical size. The most relevant mechanisms for this behaviour in advanced ceramics at low and intermediate temperatures are sub-critical crack growth (SCCG) and, to a lesser extent, cyclic fatigue. The engineering aspects of these mechanisms will be the focus of this section. Creep and corrosion will not be treated here.

6.1. Life Time and Influence of SCCG on Strength

Data for SCCG are rare. Examples of crack velocity vs. stress intensity ($v - K$) curves as determined by the method proposed by Fett and Munz [98] are shown in **Figure 14**. It can be recognised that the data follow a power law, i.e. a Paris type law for the crack growth rate is empirically observed (in fact several different crack growth mechanisms occurs, which cause a more structured $v - K$ curve, but for the technically relevant velocity region, namely the range between 10^{-13} to 10^{-6} m s^{-1}, a Paris type law can be used [39, 41, 88, 99]):

$$v = v_0 \left(\frac{K}{K_c} \right)^n \quad , \tag{21}$$

where v_0 and the SCCG exponent n are (temperature dependent) material parameters. The data in **Figure 14** were generated in laboratory air. An influence of the humidity on the crack growth rate has been reported elsewhere [39-41].

The tests on silicon nitride (the ESIS reference testing material), **Figure 14a**, were performed at several different temperatures (for details see [88]). It can be seen that the crack growth rate significantly increases, if the temperature reaches or exceeds the softening temperature of the glassy grain boundary phase. Also shown are data determined on a commercial alumina ceramic [99], **Figure 14b**. The SCCG exponent at room temperature is $n \approx 33$ for the alumina ceramic and $n \approx 50$ for the silicon nitride respectively. For ceramic materials which do not have a glassy grain boundary phase it may be even higher. For example, values around $n \approx 200$ are reported for silicon carbide ceramics [100]. The high number of the exponent suggests a loading situation of either negligible or very fast crack growth, causing failure within fractions of a second and with an extremely small transition region in between.

But more detailed analysis shows that SCCG may have a significant influence on strength in a wide range of loading conditions. This point will be discussed in the next sections in more detail.

For simplicity, in the following discussion, a general uniaxial stress state is assumed. Of course, generalisations as made in the section above (equivalent stress, effective volume, etc.) are also possible in the case of delayed fracture.

The SCCG data shown in this section have been determined experimentally. Static and constant stress rate strength tests have been performed on standard bend specimens ($3 \times 4 \times 45$ mm^3) of a commercial 99.7 % Al_2O_3 (Frialit-Degussit F99,7 by Friatec AG, D-68229 Mannheim, BRD) in 4-point flexure [99]. All experiments were conducted at room temperature in laboratory air.

The growth of cracks under load causes a finite life time of loaded specimens or components: the crack grows from its initial length a_i to the critical (final) length $a_c = a_f$. Then fast failure occurs.

The life time can be determined in the following way. The crack growth rate is the change of the crack length with time: $v = da / dt$. Then the differential of the time is $dt = (1/v) \cdot da$. Integration is possible by separation of variables. Using eq. 21 and eq. 3 gives:

$$\int_{t_i}^{t_f} \sigma^n dt = \frac{1}{v_0} \int_{a_i}^{a_c} \left(\frac{K_c}{Y\sqrt{\pi a}} \right)^n da \quad . \tag{22}$$

Here the time dependent variables are written on the left hand side and all crack length dependent variables on the right hand side of the equation. The life time, t_f, is composed of the incubation time, t_i, to originate a crack (of size a_i) and the time required for this crack to grow to its critical size ($t_f - t_i$). In ceramic processing, defects exist which behave like cracks (see previous sections). Therefore the incubation time is, in general, negligible. Exceptions are cases where cracks come to existence during the operation of the component (e.g. by impact or by corrosion).

(a)   (b)
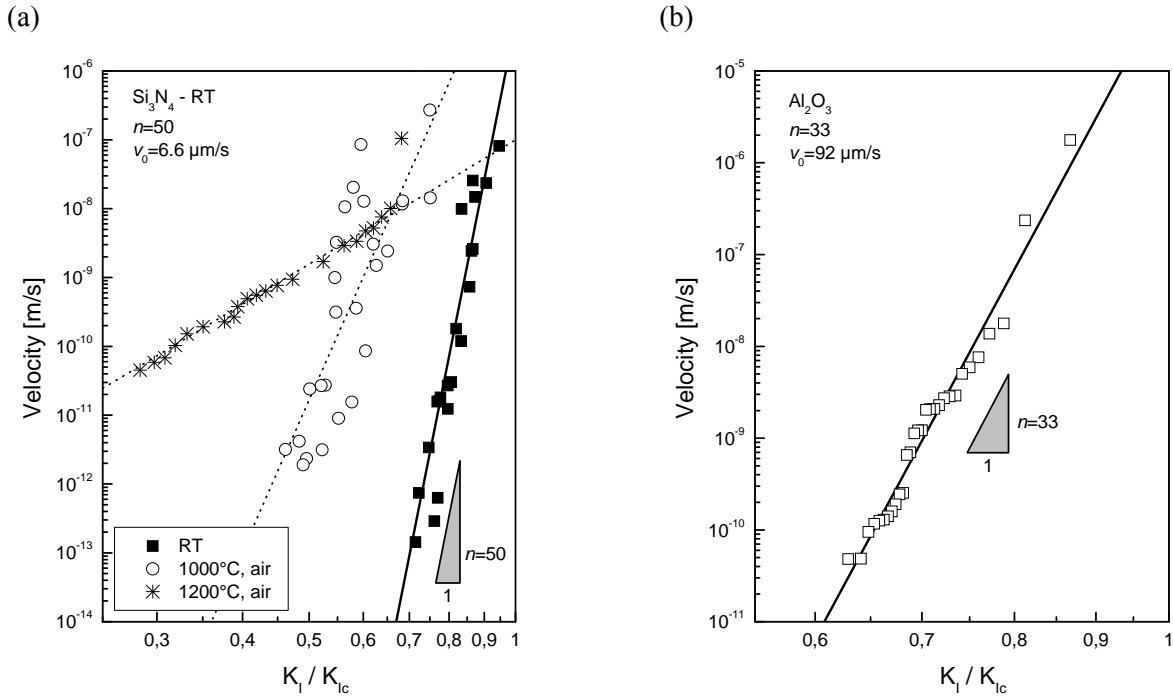
Figure 14: Crack growth rate versus stress intensity factor for a) a silicon nitride [88] and b) for an alumina ceramic [99] in a log-log representation. The data are arranged along a straight line, which indicates a power law dependency of growth rate from the stress intensity factor. At higher temperatures the crack growth rate is temperature dependent.

The geometric factor Y depends, in general, on the crack length. But if the cracks are very small compared to the dimensions of the specimen, and for slowly varying stress fields, this dependence is weak and can be neglected (this is generally the case for ceramics). An analytical integration of the right hand side of eq. 22 thus becomes possible. For $n > 2$ it holds:

$$\int_0^{t_f} \sigma(t)^n dt = \frac{2}{n-2} \cdot \frac{1}{v_0} \left(\frac{K_c}{Y\sqrt{\pi}} \right)^n \cdot \left[a_i^{(2-n)/2} - a_c^{(2-n)/2} \right] \quad . \qquad (23)$$

The right hand side of eq. 23 is a constant value. Therefore, the strength dependency of life time results from the left hand side of eq. 23. The life time strongly depends on the applied stress, because n is generally a high number. For $n \gg 1$ a rough approximation gives: $t_f \propto \sigma^{-n}$ (e.g. for $n = 33$ a stress reduction of 10 % causes a 32-fold increase in life time). For materials with a higher SCCG exponent, this influence is even more pronounced. Therefore a reduction of the applied stresses is a favourable method to increase the life time in service.

27

Of course the load spectrum (the function $\sigma(t)$ in eq. 23) can have any dependency on time. The life time t_f of the component is the upper integration limit of the integral on the right hand side: the integration over the loading spectrum has to be performed up to the time where the integral equates to the right hand side. To understand the general consequences of SCCG on fracture two simple cases will be discussed in the following.

6.1.1. Delayed Fracture under Constant Load

Delayed fracture under constant load may occur in service, e.g. in components operating for a long time under stationary loading conditions. Delayed fracture occurs without any warning, since the growth of cracks only causes a very small and therefore negligible increase in a component's compliance. A thorough theoretical understanding of the consequences of SCCG is, therefore, of great significance for design. Now we shall analyse the simple case of a test under constant load (with homogeneous and uniaxial stress state σ_{stat}). In this case and for $t_i = 0$, it can be shown, that eq. 23 becomes

$$ t_f = \frac{2}{n-2} \cdot \frac{a_i}{v_i} \cdot \left[1 - \frac{a_c}{a_i} \cdot \frac{v_i}{v_f} \right] \quad , \tag{24} $$

with $v_i = v(K_i)$, $v_f = v(K_f) = v_0$, $K_i = \sigma_{stat} Y \sqrt{\pi a_i}$ and $K_f = \sigma_{stat} Y \sqrt{\pi a_c} = K_c$ respectively.

It should be noted that the second term in the square bracket can be neglected, if any significant crack growth occurs. This is a consequence of the high value of the SCCG exponent n. For example for $a_c \geq 1.2 \cdot a_i$ and $n = 33$, this term is smaller than $0.06 \ll 1$. Then, the time to failure only depends on crack length and crack velocity at the beginning of the experiment and on the SCCG exponent.

With eq. 21 the dependence of the life time on the initial crack size can be evaluated. It is:

$$ t_f \propto a_i^{-(n-2)/2} \cdot \sigma_{stat}^{-n} \quad . \tag{25} $$

This underlines the high significance of the size of the initial cracks (and, of course, of the stress), which may grow in operation to a critical size. The life time of a specimen containing a crack 20 % larger than a reference crack is decreased by a factor 0.06, 0.01 or 10^{-8}, for a SCCG exponent of $n = 33$, 50 or 200 respectively. To reduce the size of the flaws which can transform into growing cracks is, from the manufacturer's point of view, the most effective way to improve the life time of components by the optimisation of microstructure.

The crack length at any given time under load (at constant stress) can be determined by integrating the crack growth rate over time. The result is:

$$ a(t) = a_i \left[1 - \frac{n-2}{2} \cdot \frac{v_i}{a_i} \cdot t \right]^{2/(2-n)} \tag{26a} $$

or

$$ a_i = a \left[1 + \frac{n-2}{2} \cdot \frac{v}{a} \cdot t \right]^{2/(2-n)} \tag{26b} $$

This function is plotted in **Figure 15a** for $n = 33$, 50 and 200 for alumina, silicon nitride and silicon carbide respectively, using the same material properties at a load level of $\sigma_{stat} / \sigma_i = 0.95$ with $\sigma_i = K_c / (Y \sqrt{\pi a_i})$ and $Y = 2/\pi$. The disproportionate influence of the SCCG exponent can easily be recognised. Due to the high value of this exponent, the crack needs a large part of its life to grow the first few percent. Then the crack growth rate accelerates to such an extent that failure occurs in a very short fraction of the life time. Of course the growth rate of cracks strictly depends on the initial crack size **Figure 15b**.

(a)   (b)
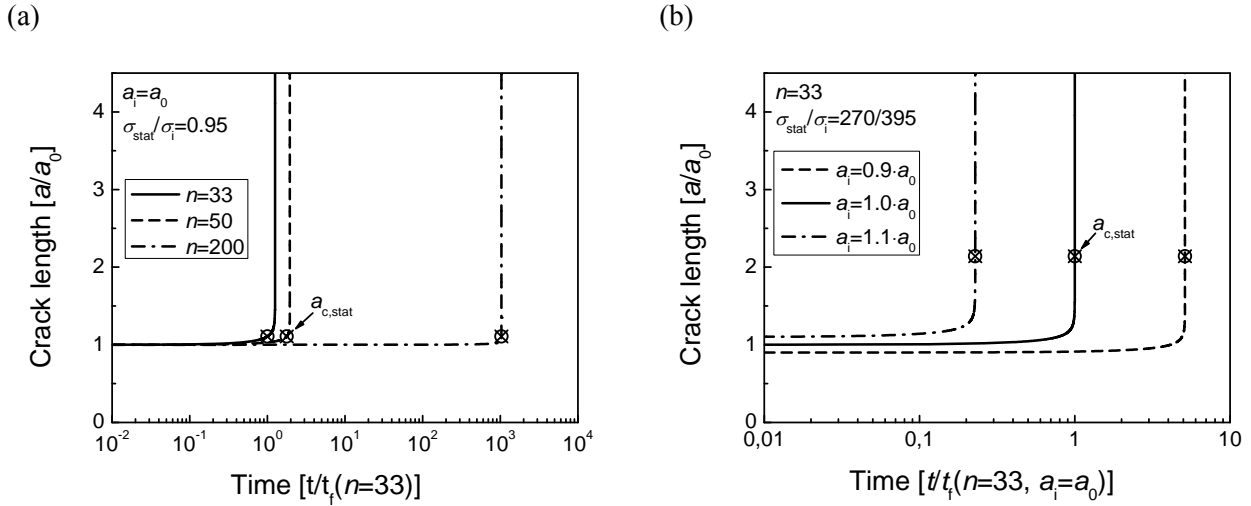
Figure 15: Crack length versus time for a) materials having a different SCCG exponent n (used are data of alumina, silicon nitride and silicon carbide respectively, $\sigma_{stat} / \sigma_i = 0.95$) and b) for cracks of different initial size (used is the SCCG exponent of alumina). The cracks need a large fraction of specimen life time to grow the first few percent. They then accelerate and fracture occurs very quickly. This behaviour is promoted by high SCCG exponents.

The large influence of the initial flaw size on life time can be studied with a series of constant stress tests. **Figure 16a** shows the test results of 4-point bending tests at constant load ($\sigma = 395$ MPa, testing conditions and specimen geometry according to EN 843-1 [82]) performed on the alumina ceramic described above. The data (30 tests) are plotted as a Weibull graph (cumulative frequency versus life time). The measured life time ranges from around 10 s to almost 10^6 s. Also shown, in **Figure 16b**, is the Weibull distribution of the material, which has been determined in conventional 4-point bending tests according to EN 843-1 [82]. Of course the scatter of data in both distributions is a result of the specimen to specimen variation in the size of the critical flaw. Therefore, the "time Weibull distribution" can be deduced from the "strength Weibull distribution" (eq. 12) by taking SCCG into account.

Strength and crack size are related by the failure criterion (see for example eq. 9) and the change of crack length with time is described by eq. 26. By use of eq. 26 and eq. 9 the Weibull distribution becomes time dependent [2, 4, 14]:

$$F\left(\sigma_{stat}, V, t\right) = 1 - \exp\left[-\frac{V}{V_0} \left(\frac{\sigma_{stat}}{\sigma_0} \right)^m \left(\frac{\sigma_{stat}^2}{C} t + 1 \right)^{m/(n-2)} \right] \quad , \quad (27)$$

where the constant $C = 2K_c^2 / (\pi Y^2 v_0 (n-2))$ is a material and geometry dependent parameter. The crack growth rate at fracture is $v_f = v_0$. If only little SCCG occurs, $\sigma_{stat}^2 t / C << 1$ and eq. 27 becomes equal to eq. 12. If SCCG is significant, $\sigma_{stat}^2 t / C >> 1$, we get the time Weibull distribution:

$$F(\sigma_{stat}, V, t) \approx 1 - \exp[-\frac{V}{V_0} \cdot \left(\frac{t}{t_0(\sigma_{stat})}\right)^{m^*}] \qquad (28)$$

with

$$t_0(\sigma) = \frac{C}{\sigma_{stat}^2} \left(\frac{\sigma_0}{\sigma_{stat}}\right)^{(n-2)} \quad , \qquad (29)$$

and

$$m^* = \frac{m}{n-2} \quad . \qquad (30)$$

The time Weibull modulus only depends on the slope of the flaw distribution (which is given by the Weibull modulus and the SCCG exponent).

Its obvious that n can be determined by measurement of m and m^*. In the case of the investigated alumina [99], $m = 17$ and $m^* = 0.55$. The resulting SCCG exponent is $n \approx 33$.

A comprehensive way of representing design data is the strength – probability – time (SPT) diagram, which was developed about 30 years ago [2, 101]. In these diagrams, eq. 28 is used to design Weibull diagrams (failure probability versus strength - for an example see Figure 8), for a constant time to failure. Of course the other design parameters (equivalent stress, effective volume) should also be properly accounted for.

A more detailed analysis of both types of Weibull distribution enables the determination of $v - K$ curves for crack growth without any special assumptions with regard to its analytical form [98]. In fact, the crack growth data shown in **Figure 14b** have been determined using such an analysis of the data shown in **Figure 16a**. The straight line in the diagram is a fit through the data giving $n \approx 33$.

6.1.2. Delayed Fracture under Increasing Load: Constant Stress Rate Tests

SCCG also influences loading situations in which the stress is not constant. A simple example is a test where the stress increases linearly with time (constant stress rate test: $\sigma = \dot{\sigma} \cdot t$). In this case also the left hand side of eq. 23 can be integrated analytically. After some rearrangement of the formulae we get:

$$\sigma_f^{n+1} = \frac{2(n+1)}{n-2} \cdot \frac{a_i}{v_0} \cdot \sigma_i^n \cdot \dot{\sigma} \left[1 - \left(\frac{\sigma_f}{\sigma_i}\right)^{n-2}\right] \quad , \qquad (31)$$

where $\sigma_i = K_c / (Y\sqrt{\pi a_i})$ is the inert strength (i.e. the strength of the specimen without any SCCG) and σ_f is the strength of the specimen after some SCCG. Of course $\sigma_f \leq \sigma_i$. Again, if any significant SCCG occurs, the second term in the square bracket is very small compared to unity and can be neglected. Then the strength of specimens tested with a constant stress rate then depends on the stress rate: $\sigma_f \propto \dot{\sigma}^{1/(n+1)}$. This behaviour can be recognised in **Figure 17**, where constant stress rate test results on alumina are shown.

Presented is the strength versus stress rate in a log-log plot. For "low" stress rates $\sigma_f \propto \dot{\sigma}^{1/(n+1)}$ with a fit to the data yields $n \approx 33$. Note the consistancy of the SCCG-exponent determined with different methods. For stress rates higher than $\sim 10^2$ MPa·s^{-1} the testing time is too short for significant SCCG and the strength is equal to the inert strength. It should be noted that for conventional bending tests on the analysed alumina according to EN 843-1 [82] the testing velocity is high enough that significant SCCG does not occur. So the determined strength is (almost) equal to the inert strength.

(a)   (b)
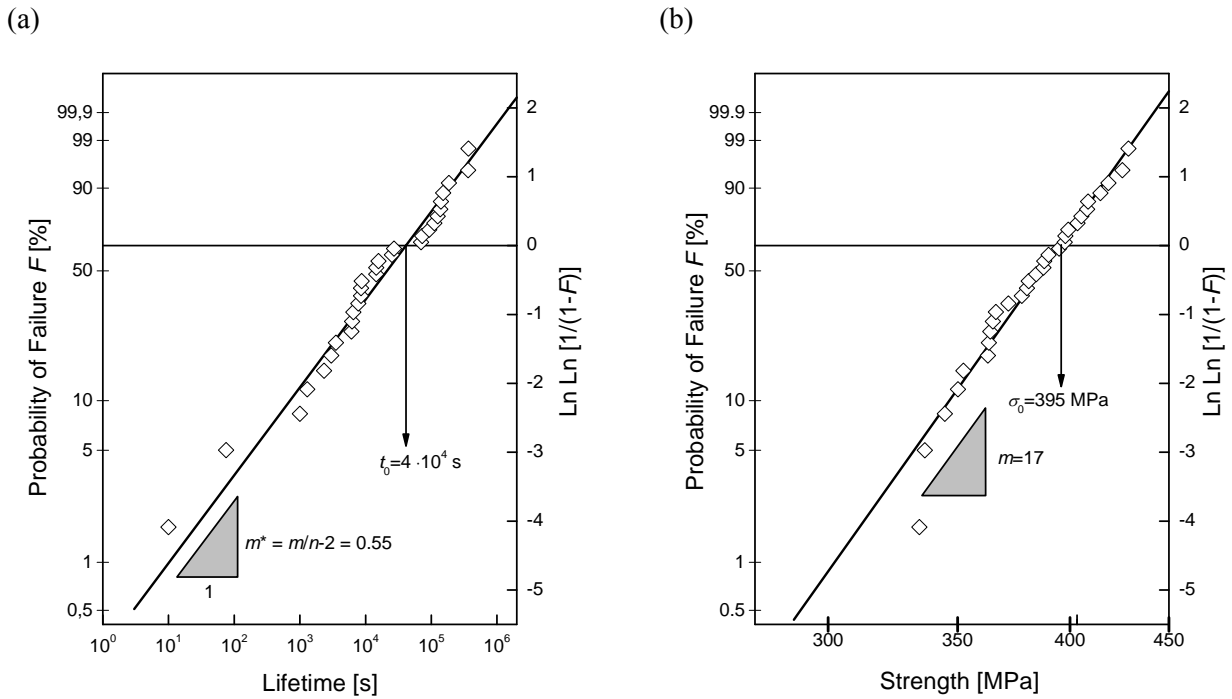
Figure 16: Bending tests at room temperature on an alumina ceramic [99]. Plotted is the cumulative frequency a) versus time to failure for constant loading ($\sigma = 270$ MPa) and b) versus strength for tests according to EN 843-1 (i.e. inert strength). A comparison of both types of test makes the determination of the crack growth curve ($v - K$ -curve) possible.
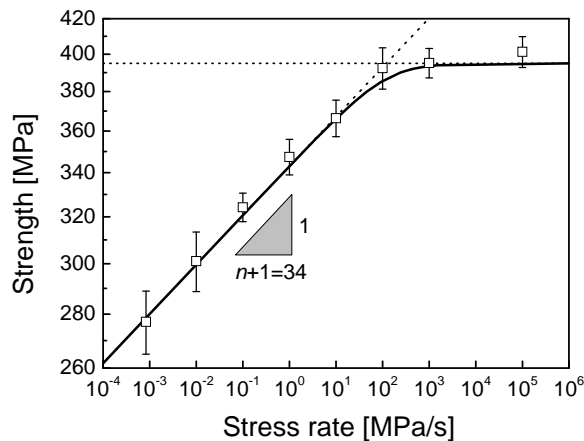
Figure 17: (Mean) strength versus stress rate for constant stress rate tests performed on alumina (same material as described above). For details see [99]. The SCCG exponent determined using this data is $n = 33$. Each data point results from 7 (and in one case from 30) individual measurements. The scatter bars reflect the 90 % uncertainties due to the sampling procedure, which are much smaller for the characteristic strength than for the Weibull modulus.

In summary, two loading regions can be recognised: at low stress rates a strong influence of SCCG on the strength exists; at (very) high rates SCCG has no significant influence on the strength. In both regions, the strength is controlled by the size and distribution of flaws. As discussed in the previous section, this situation must be described by statistical means.

6.1.3. Delayed Fracture under General Loading Conditions

In reality, multi-axial inhomogeneous stress fields, which vary with time, occur in components. Delayed fracture due to SCCG is, in general, accounted for on the basis of eq. 22. Methods to consider the influence of inhomogeneous and multi-axial stress fields have been discussed in the previous sections. Thus all necessary tools for proper design against delayed fracture in brittle materials are available. A few examples for the application of such design methodology can be found in literature [101, 102].

6.2. Influence of Fatigue Crack Growth on Strength

Although cyclic fatigue has been recognised to be a possible damage mechanism in ceramics, almost no cyclic fatigue data exists for engineering ceramics [43, 103-106]. A rare exception is the data of NGK Insulators Ltd. on their silicon nitride material [107]. It follows from the reported cyclic fatigue data that there also exists a Paris law for cyclic fatigue crack growth. The crack growth per load cycle is

$$\frac{da}{dN} = \left(\frac{\Delta a}{\Delta N}\right)_0 \left(\frac{\Delta K}{K_c}\right)^{\tilde{n}} \quad . \tag{32}$$

The material parameters, the factor $(\Delta a / \Delta N)_0$ and the Paris exponent $\tilde{n}$, are dependent on mean stress and temperature. N is the number of load cycles and N_f is the numbers of cycles to failure.

Cyclic crack growth influences life-time in an similar manner to SCCG (see previous section). Under conditions where cyclic fatigue is the dominating damage mechanism, the cyclic life-time can be determined in an analogous way to the procedures discussed above. For example, the equation analogous to eq. 27 is [14]:

$$F(\sigma, V, N_f) = 1 - \exp\left[-\frac{V}{V_0}\left(\frac{\Delta\sigma}{\sigma_0}\right)^m \left(\frac{\Delta\sigma^2}{\Delta C} N_f + 1\right)^{m/(\tilde{n}-2)}\right] \quad , \tag{33}$$

where ΔC is a material parameter which is defined in an similar way to the parameter C.

It should be noted that in the few cases reported, the SCCG exponent for cyclic fatigue is much larger than unity: $\tilde{n} \gg 1$ [105, 108, 109]. Thus, like SCCG, cyclic fatigue life is strongly dependent on the applied stress range and the size of the initial flaws.

The action of cyclic fatigue and of SCCG can be assumed to be independent and the crack advance due to both mechanisms can be simply added. But since both growth rates strongly depend on the applied load and since the SCCG exponents are, in general, different, it is quite likely that the growth rates are very different. Then the simplified model description can be used that only one of both mechanisms is dominating.

6.3. Proof Testing

Proof testing is an often (routinely) used technique to guarantee a component's minimum service life [2, 4, 110, 111]. To make the basic ideas of proof testing clearer, we relate again to a uniaxial tensile and homogeneous stress state.

In a proof test the component is loaded with a stress σ_p, which is higher than the design service stress σ_a.

The critical flaw size in a proof test is $a_c(\sigma_p) = (1/\pi) \cdot (K_c / Y\sigma_p)^2$. In a proof test all components containing equal or larger sized flaws are destroyed. In other words, the frequency distribution of flaws is truncated at $a \leq a_c(\sigma_p)$.

The critical crack size in service is $a_c(\sigma_a) = (1/\pi) \cdot (K_c / Y\sigma_a)^2$ and $a_c(\sigma_p) < a_c(\sigma_a)$. If the crack growth law is known, the time can be determined that the crack needs to grow from $a_c(\sigma_p)$ to the critical size $a_c(\sigma_a)$.

If SCCG is the dominating damage mechanism, this can be calculated on the basis of eq. 26 with $a_i = a_p$ and $a = a_a$. Then, the time $t = t_{a,min}$ is the shortest possible time for a crack in a component to grow to a critical size. Thus the time $t_{a,min}$ is the life-time which can be guaranteed for a proof tested component. This procedure can be used to determine a suitable proof stress if the loading stress and the crack growth law are known. In practice, however, neither the loading stress nor the crack growth law are precisely known. Consequently, proof testing is often done at much too high stresses, which results in an unnecessarily large proportion of rejections.

It is often claimed that proof testing causes damage in the component. Of course, any applied stress causes some SCCG, thereby reducing the remaining strength. But if the stress rate during proof testing is high enough, this loss of strength can be neglected. Therefore, the loading rate and especially the unloading rate in proof tests should be high. If, for any reason, the application of a high loading rate in a proof test is not possible, the elongation of cracks during testing can be estimated and accounted for. Thus the reliability of surviving parts can still be guaranteed.

An often occurring problem is that the in-service stress fields of components cannot easily be simulated in a test. For example, the stress fields caused by temperature changes or by contact loading can hardly be reproduced in simple mechanical tests. In such cases, large parts of a component are often subjected to a too large a proof stress, which increases the number of failures in the test. On the other hand, some parts of a component are subjected to too small proof a stress. The proof test then only reduces the failure probability, but some in-service failure are still possible.

If cyclic fatigue is the dominating crack growth mechanism of cracks, the above arguments can be used in an analogous way.

7. Concluding Remarks

Over the past few sections we have looked closely at the phenomenon of fracture in ceramics. We have analysed the macroscopic appearance of fracture and typical failure modes in ceramic materials, identified fracture mirrors and fracture origins and have seen how fracture is intrinsically connected to the

microstructure of a ceramic and the detail of stress distributions and recognised that fracture always starts at a single microstructural flaw, the stability of which can be described with simple linear elastic fracture mechanics.

These features are responsible for the inherent statistical nature of failure in ceramic materials. However, by understanding this, we have been able to treat the statistics of fracture, to understand the close correlation between defect populations and fracture statistics and have seen how we can develop materials parameters, e.g., the characteristic strength, the Weibull modulus or effective volume to help us plan and design appropriately for such material behaviour.

The influence of different damage mechanisms has been discussed and related to their effect in design. In particular, environmental and time (delay) effects have been analysed. Subcritical crack growth has been recognised to be the most significant damage mechanism for the delayed failure of components and the huge influence of the initial flaw (crack) size on the life time has been demonstrated on examples. Finally a tool for dealing with these (proof testing) has been discussed.

Of course, it can not be claimed that this short treatise is in any way comprehensive and several important points have not been dealt with in the detail they would deserve, e.g. aspects related to toughness [3, 4, 61, 112, 113] and the increase of toughness with crack growth (R-curve behaviour [3, 4, 114, 115]), the influence of internal stresses on toughness [116, 117] and strength [118, 119], or all aspects related to layered materials [120-123], graded materials [124] and composites. Each of these topics, and several others, would be worthy of a separate section by themselves. Nevertheless, the basic concepts have been presented and tools for handling them have been provided.

Today fracture mechanics of ceramics is used to large extent for the analysis of fractured components [17]. Dangerous loading conditions can be recognised and reasons for failing such as improper use [17], bad mechanical design [110], imperfect materials processing [19, 125], or inadequate materials selection can be identified. In some cases even the local fracture stress can be read from the fracture surface [16, 21, 126]. Thus the fractographic analysis is very often a powerful tool to recognise the weak point in the system and gives clear advice for possible improvements [19]. However, although numerical design tools for the application of fracture statistical methods and methods for life time prediction are commercially available [74, 75], and although they are definitely needed for a proper mechanical design process, they are almost not used in the daily design practice. The reasons for that behaviour are manifold, e.g. the complexity of the methods, inadequate training of ceramic engineers in numerical mathematics, deficiencies in education or a lack of appropriate material data [13, 89]. But increasingly high technical demands, the increasing need for the use of technical ceramics for highly loaded applications and the generally increased acceptance of numerical simulation methods will certainly cause a higher recognition and application of these methods in the near future.

Although the largest and indeed fastest growing part of ceramic applications exploits their functional and not their structural properties [127-131], e.g., in electronic or micromechanical devices, failure, in the final instance, is still a frequent mechanical event and poor mechanical properties are quite often limiting their application. This is a serious but not well recognised problem. Several orders of magnitude more fractures occur in functional as in structural ceramic parts but work about the their mechanical behaviour is in its infancy. [26, 132-138]. To give some examples' thermal strains and stresses are causing fracture of microelectronic components, large strains and stresses are triggered in future fuel injection systems by piezoelectric ceramic materials, and positive temperature resistors suffer from large thermomechanical strains due to a functionally necessary phase transformation. The concepts, mechanisms and tools we have discussed remain as valid for these components as for any structural parts. This can be symbolised by the two fracture origins shown in **Figure 18**. Presented are fractures of commercial PTC components. The left one shows a fracture surface of a barium titanate PTC component after an over voltage loading and right one the fracture surface of a bending test specimen cut out of the PTC. On the fracture surfaces no significant

differences can be detected, but one fracture occurred due to a too high electrical load and the other due to a too high mechanical load.

(a) (b)
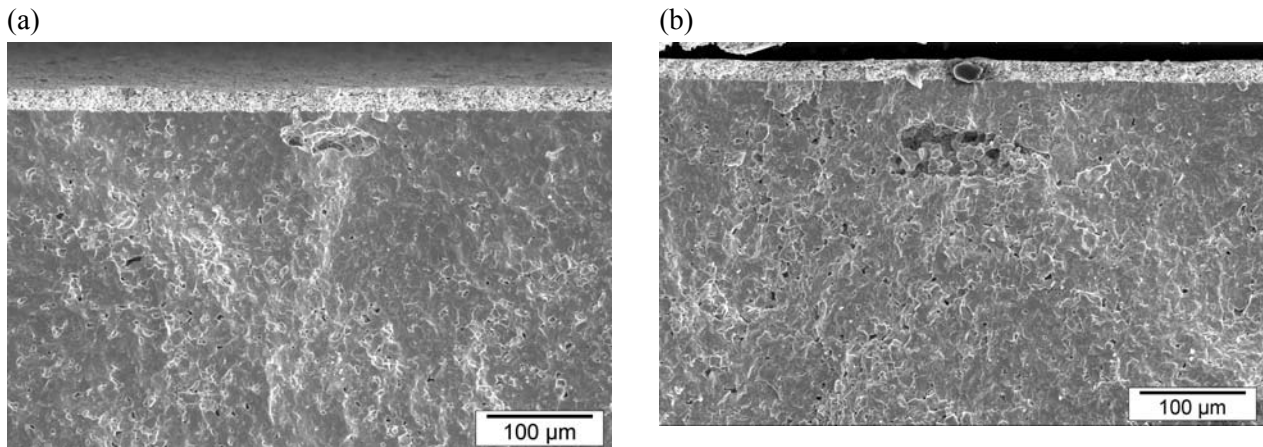
Figure 18: a) Fracture surface in a thermistor component after over voltage loading and b) in a bending test specimen made of the same barium titanate ceramic. Qualitative differences between both types of fracture surfaces can hardly be recognised.

The great challenge for the future will be the generation, acquisition and collection of valid materials data for the economically increasingly important group of functional ceramic materials and of the development of a clear understanding of the corresponding fracture mechanisms.

8. References

[1] D. W. Kingery, H. K. Bowen, D. R. Uhlmann, *Introduction to Ceramics*, John Wiley & Sons, New York, **1976**.

[2] R. W. Davidge, *Mechanical Behaviour of Ceramics*, Cambridge University Press, Cambridge, **1979**.

[3] J. B. Wachtman, *Mechanical Properties of Ceramics*, Wiley-Interscience, New York, Chichester, **1996**.

[4] D. Munz, T. Fett, *Ceramics*, Springer, Berlin, Heidelberg, **1999**.

[5] H. Hertz, *J. reine. angew. Math.* **1882,** 92, 156.

[6] ISO 14704:**2000,** *Fine Ceramics (Advanced Ceramics, Advanced Technical Ceramics) - Test Method for Flexural Strength of Monolithic Ceramics at Room Temperature*.

[7] R. Danzer, T. Lube, in: *Tagungsband Werkstoffprüfung*, (Ed: M. Pohl), Werkstoff-Informationsgesellschaft mbH, Frankfurt, **2004,** 245.

[8] EN ISO 18756:**2003,** *Fine ceramics (Advanced Ceramics, Advanced Technical Ceramics) - Determination of FractureToughness of Monolithic Ceramics at Room Temperature by the Surface Crack in Fexure (SCF) Method*.

[9] ISO 24370:**2005,** *Fine Ceramics (Advanced Ceramics, Advanced Technical Ceramics) – Determination of Fracture Toughness of Monolithic Ceramics at Room Temperature by the Chevron-notched Beam (CNB) Method*.

[10] ISO DIS 23146:**2007,** *Fine Ceramics (Advanced Ceramics, Advanced Technical Ceramics) – Determination of Fracture Toughness of Monolithic Ceramics at Room Temperature by the Single-edge Vee-notched Beam (SEVNB) Method*.

[11] R. J. Primas, R. Gstrein, *Fat. Fract. Engng. Mater. Struct.* **1997,** 20, 513.

[12] EN ISO 15732:**2003,** *Fine ceramics (Advanced Ceramics, Advanced Technical Ceramics) - Determination of FractureToughness of Monolithic Ceramics at Room Temperature by the Single-edge Pre-cracked Beam (SEPB) Method.*

[13] T. Lube, R. Danzer, M. Steen, in: *Improved Ceramics Through New Measurements, Processing and Standards*, (Eds: M. Matsui, S. Jahanmir, H. Mostgaci, M. Naito, K. Uematsu, R. Waesche, R. Morrell), The American Ceramic Society, Westerville, **2002,** 259.

[14] R. Danzer, in: *The Encyclopedia of Advanced Materials*, (Eds: D. Bloor, R. J. Brook, M. C. Flemings, S. Mahajan, R. W. Cahn), Pergamon, **1994,** 385.

[15] T. Lube, *Entwicklung eines Zugversuches zur Zuverlässigkeitsprüfung von keramischen Ventilen*, Diplomarbeit am Institut für Metallkunde und Werkstoffprüfung, Montanuniversität, **1993,** 89.

[16] J. J. Mecholsky, *Ceram. Trans.* **1991,** 17, 413.

[17] R. Morrell, *Fractography of Brittle Materials*, National Physical Laboratory, Teddington, **1999**.

[18] CEN/TS 843-6:**2004,** *Advanced Technical Ceramics - Monolithic Ceramics. Mechanical Properties at Room Temperature - Part 6: Guidance for Fractographic Investigation*.

[19] R. Danzer, *Key Eng. Mat.* **2002,** 223, 1.

[20] ASTM C 1322-05b:**2005,** *Standard Practice for Fractography and Characterization of Fracture Origins in Advanced Ceramics*.

[21] R. Morrell, L. Byrne, M. Murray, in: *Fractography of Glasses and Ceramics IV*, (Eds: J. R. Varner, G. D. Quinn, V. D. Frèchette), The American Ceramic Society, Westerville, **2001,** 253.

[22] K. D. Mörgenthaler, E. Tiefenbacher, *Abschlußbericht des 3.Förderungszeitraumes (1.3.1980 bis 30.6.1983) zum Forschungsvorhaben "Bauteile aus Keramik für Gasturbinen" (ZK/NT/NTS1021), BMFT-FB-T 86 027*, Fachinformationszentrum Karlsruhe, , Karlsruhe, **1983**.

[23] K. D. Mörgenthaler, in: *Technische Keramik Jahrbuch*, Vulkan-Verlag, Essen, **1988,** 285 .

[24] D. P. H. Hasselman, *J. Am. Ceram. Soc.* **1969,** 52, 600.

[25] G. A. Schneider, R. Danzer, G. Petzow, *Fortschr.ber. DKG* **1988,** 3, 59.

[26] P. Supancic, R. Danzer, *Ceram. Eng. Sci. Proc.* **2003,** 24, 371.

[27] M. Fellner, P. Supancic, *Key Eng. Mat.* **2002,** 223, 97.

[28] B. R. Lawn, *J. Am. Ceram. Soc.* **1998,** 81, 1977.

[29] M. Lengauer, R. Danzer, *J. Eur. Ceram. Soc.* **submitted 2007**, .

[30] M. Lengauer, R. Danzer, W. Harrer, in: *Walzen mit Keramik*, (Eds: A. Kailer, T. Hollstein), Fraunhofer IRB Verlag, Stuttgart, **2004,** 95.

[31] T. Lube, *J. Eur. Ceram. Soc.* **2001,** 21, 211.

[32] S. Jahanmir, *Friction and Wear of Ceramics*, Marcel Dekker, New York, **1994**.

[33] N. J. McCormick, E. A. Almond, *J. Hard Mat.* **1990,** 1, 25.

[34] R. Morrell, *Key Eng. Mat.* **2005,** 290, 14.

[35] R. Danzer, M. Hangl, R. Paar, in: *Fractography of Glasses and Ceramics IV*, (Eds: J. R. Varner, G. D. Quinn, V. D. Frèchette), The American Ceramic Society, Westerville, **2001,** 43.

[36] H. Chai, B. R. Lawn, *Int. J. Fract.* **2007,** 145, 159.

[37] J. B. Quinn, in: *Fractography of Glasses and Ceramics V*, (Eds: J. R. Varner, G. D. Quinn, M. Wightman), Wiley-Interscience, Hoboken, **2007,** 253.

[38] G. Schoeck, *Int. J. Fract.* **1990,** 44, 1.

[39] S. M. Wiederhorn, *J. Am. Ceram. Soc.* **1967,** 50, 407.

[40] T. A. Michalske, S. M. Freiman, *Nature* **1982,** 95, 511.

[41] R. Danzer, in: *The Encyclopedia of Advanced Materials*, (Eds: D. Bloor, R. J. Brook, M. C. Flemings, S. Mahajan, R. W. Cahn), Pergamon, **1994,** 2693.

[42] R. K. Dauskardt, W. Yu, R. O. Ritchie, *Eng. Mat. Struct.* **1997,** 20, 1453.

[43] C. J. Gilbert, R. O. Ritchie, *J. Am. Ceram. Soc.* **1987,** 70, C248.

[44] G. Grathwohl, T. Liu, *J. Am. Ceram. Soc.* **1991,** 74, 318.

[45] A. M. Brown, M. F. Ashby, *Acta Met.* **1980,** 28, 1085.

[46] H. J. Frost, M. F. Ashby, *Deformation Mechanism Maps*, Pergamon Press, Oxford, **1982**.

[47] H. Riedel, *Fracture at High Temperatures*, Springer-Velag, Berlin, **1987**.

[48] K. G. Nickel, Y. G. Gogotsi, in: *Handbook of Ceramic Hard Materials*, (Ed: R. Riedel), VCH-Wiley, Weinheim, **2000,** 140.

[49] B. Schneider, A. Guette, R. Naslain, M. Cataldi, A. Costecalde, *J. Mater. Sci.* **1998,** 33, 535.

[50] A. B. Alles, V. L. Burdick, *J. Am. Ceram. Soc.* **1993,** 76, 401.

[51] B. R. Lawn, *Fracture of Brittle Solids - Second Edition*, Cambridge University PRess, Cambridge, **1993**.

[52] S. P. Timoshenko, J. N. Goodier, *Theory of Elasticity*, McGraw-Hill, New York, **1970**.

[53] D. Gross, T. Seelig, *Fracture Mechanics*, Springer, Berlin, **2006**.

[54] Y. Murakami, *The Stress Intensity Factor Handbook*, Pergamon Press, New York, **1986**.

[55] H. Tada, P. Paris, G. R. Irwin, *The Stress Analysis Handbook*, Del Research Corporation, St. Louis, **1985**.

[56] J. C. Newman, I. S. Raju, *Eng. Fract. Mech.* **1981,** 15, 185.

[57] A. A. Griffith, *Phil. Trans. Royal Soc. London* **1920,** A221, 163.

[58] A. G. Evans, *J. Am. Ceram. Soc.* **1990,** 73, 187.

[59] Y.-M. Mai, B. R. Lawn, *J. Am. Ceram. Soc.* **1987,** 70, 289.

[60] P. L. Swanson, C. J. Fairbanks, B. R. Lawn, Y.-M. Mai, B. J. Hockey, *J. Am. Ceram. Soc.* **1987,** 70, 279.

[61] R. W. Steinbrech, O. Schenkel, *J. Am. Ceram. Soc.* **1988,** 71, C271.

[62] R. Danzer, *J. Eur. Ceram. Soc.* **2006,** 26, 3043.

[63] A. Zimmermann, M. Hoffmann, B. D. Flinn, R. K. Bordia, T.-J. Chuang, E. R. Fuller, J. Rödel, *J. Am. Ceram. Soc.* **1998,** 81, 2449.

[64] C. Lu, R. Danzer, F. D. Fischer, *J. Eur. Ceram. Soc.* **2004,** 24, 3643.

[65] R. Danzer, *J. Eur. Ceram. Soc.* **1992,** 10, 461.

[66] R. A. Hunt, L. N. McCartney, *Int. J. Fract.* **1979,** 15, .

[67] A. d. S. Jayatilaka, K. Trustrum, *J. Mater. Sci.* **1977,** 12, 1426.

[68] L. N. McCartney, *Int. J. Fract.* **1979,** 15, 477.

[69] R. Danzer, G. Reisner, H. Schubert, *Z. Metallkde.* **1992,** 83, 508.

[70] R. Danzer, T. Lube, P. Supancic, *Z. Metallkde.* **2001,** 92, 773.

[71] R. Danzer, P. Supancic, J. Pascual Herrero, T. Lube, *Eng. Fract. Mech.* **2007,** 74, 2919.

[72] W. Weibull, *A Statistical Theory of the Strength of Materials*, Generalstabens Litografiska Anstalts Förlag, Stockholm, **1939**.

[73] W. Weibull, *J. Appl. Mech.* **1951,** 18, 293.

[74] A. Brückner-Foit, A. Heger, D. Munz, *Ceram. Eng. Sci. Proc.* **1993,** 14, 331.

[75] N. N. Nemeth, J. M. Manderscheid, J. P. Gyekenyesi, *Am. Ceram. Soc. Bull.* **1989,** 68, 2064.

[76] G. D. Quinn, *J. Am. Ceram. Soc.* **2003,** 86, 508.

[77] G. D. Quinn, *J. Am. Ceram. Soc.* **2003,** 86, 475.

[78] A. M. Freudenthal, in: *Fracture*, (Ed: H. Liebowitz), Academic Press, New York, London, **1968,** 591.

[79] J. Lamon, *J. Am. Ceram. Soc.* **1990,** 73, 2204.

[80] T. Thiemeier, A. Brückner-Foit, H. Kölker, *J. Am. Ceram. Soc.* **1991,** 74, 48.

[81] A. Brückner-Foit, T. Fett, D. Munz, K. Schirmer, *J. Eur. Ceram. Soc.* **1997,** 17, 689.

[82] EN 843-1:**1995,** *Advanced Technical Ceramics - Monolithic Ceramics - Mechanical Properties at Room Temperature: Part 1 - Determination of Flexural Strength*.

[83] ASTM C 1161-02c:**2002,** *Standard Test Methods for Flexural Strength of Advanced Ceramics at Ambient Temperature*.

[84] JIS R 1601:**1995,** *Testing Method for Flexural Strength (Modulus of Rupture) of Fine Ceramics*.

[85] ENV 843-5:**1997,** *Advanced Technical Ceramics - Monolithic Ceramics - Mechanical Properties at Room Temperature: Part 5- Statistical Evaluation*.

[86] ASTM C 1239-95:**1995,** *Standard Practice for Reporting Uniaxial Strength Data and Estimating Weibull Distribution Paramters for Advanced Ceramics*.

[87] JIS R 1625:**1996,** *Weibull Statistics of Strength Data for Fine Ceramics*.

[88] T. Lube, R. Danzer, J. Kübler, J. Dusza, J.-P. Erauw, H. Klemm, V. M. Sglavo, in: *Fracture Beyond 2000*, (Eds: A. Neimitz, I. V. Rokach, D. Kocanda, K. Golos), EMAS Publications, Sheffield, **2002,** 409.

[89] T. Lube, J. Dusza, *J. Eur. Ceram. Soc.* **2007,** 27, 1203.

[90] A. Börger, P. Supancic, R. Danzer, *J. Eur. Ceram. Soc.* **2002,** 22, 1425.

[91] A. Börger, P. Supancic, R. Danzer, *J. Eur. Ceram. Soc.* **2004,** 24, 2917.

[92] R. Danzer, W. Harrer, P. Supancic, T. Lube, Z. Wang, A. Börger, *J. Eur. Ceram. Soc.* **2007,** 27, 1481.

[93] F. I. Baratta, M. W. T., G. D. Quinn, *Errors Associated with Flexure Testing of Brittle Materials*, U.S. Army Materials Technology Laboratory, Watertown, **1997**.

[94] T. Lube, M. Manner, R. Danzer, *Fat. Fract. Engng. Mater. Struct.* **1997,** 20, 1605.

[95] C. Lu, R. Danzer, F. D. Fischer, *Phys. Rev.* **2002,** E65, Article Number 067102.

[96] L. Sigl, *Z. Metallkde.* **1992,** 83, 518.

[97] R. Danzer, T. Lube, in: *Ceramic Materials, Components for Engines*, (Ed: K. Niihara), Japan Fine Ceramics Association, Tokyo, **1998,** 683.

[98] T. Fett, D. Munz, *J. Am. Ceram. Soc.* **1985,** 68, C213.

[99] R. G. A. Baierl, *Langsames Rißwachstum in Aluminiumoxid*, Diplomarbeit am Institut für Struktur- und Funktionskeramik, Montanuniversität Leoben, **1999,** 83.

[100] H. Richter, G. Kleer, W. Heider, R. Röttenbacher, *Mat. Sci. Eng.* **1985,** 71, 203.

[101] H. Hempel, H. Wiest, *ASME Paper No. 86-GT-199* **1986**, .

[102] T. Soma, Y. Ishida, M. Matsui, I. Oda, *Advanced Ceramic Materials* **1987,** 2, 809.

[103] T. Kawakubo, K. Komeya, *J. Am. Ceram. Soc.* **1987,** 70, 400.

[104] M. J. Reece, F. Guiu, M. F. R. Sammur, *J. Am. Ceram. Soc.* **1989,** 72, 348.

[105] C. J. Gilbert, R. H. Dauskardt, R. O. Ritchie, *J. Am. Ceram. Soc.* **1995,** 78, 2291.

[106] C. J. Gilbert, J. J. Cao, W. J. Moberlychan, L. C. DeJonghe, R. O. Ritchie, *Acta Mat.* **1996,** 44, 3199.

[107] M. Masuda, T. Soma, M. Matsui, *J. Eur. Ceram. Soc.* **1990,** 6, 253.

[108] S.-Y. Liu, I. W. Chen, *J. Am. Ceram. Soc.* **1994,** 77, 2025.

[109] R. H. Dauskardt, M. R. James, J. R. Porter, R. O. Ritchie, *J. Am. Ceram. Soc.* **1992,** 75, 759.

[110] R. Morrell, *Handbook of Properties of Technical & Engineering Ceramics, Part 1: An Introduction for the Engineer and Designer*, Her Majesty's Stationary Office, London, **1989**.

[111] T. Soma, Y. Ishida, M. Matsui, I. Oda, *Adv. Ceram. Mat.* **1987,** 2, 809.

[112] R. M. McMeeking, A. G. Evans, *J. Am. Ceram. Soc.* **1982,** 65, 242.

[113] J. Rödel, *J. Eur. Ceram. Soc.* **1992,** 9, 325.

[114] D. K. Shetty, J.-S. Wang, *J. Am. Ceram. Soc.* **1989,** 72, 1158.

[115] K. Kendall, N. M. Alford, S. R. Tan, J. D. Birchall, *J. Mat. Res.* **1986,** 1, 120.

[116] M. Lugovy, V. Slyunyayev, N. Orlovskaya, G. Blugan, J. Kübler, M. H. Lewis, *Acta Mat.* **2005,** 53, 289.

[117] T. Lube, J. Pascual Herrero, F. Chalvet, G. de Portu, *J. Eur. Ceram. Soc.* **2007,** 27, 1449.

[118] A. V. Virkar, J. L. Huang, R. A. Cutler, *J. Am. Ceram. Soc.* **1987,** 70, 164.

[119] J. Pascual Herrero, F. Chalvet, T. Lube, G. de Portu, *Mat. Sci. Forum* **2005,** 492-493, 581.

[120] H. M. Chan, *Ann. Rev. Mat. Sci.* **1997,** 27, 249.

[121] M. P. Rao, A. J. Sánchez-Herencia, G. E. Beltz, R. M. McMeeking, F. F. Lange, *Science* **1999,** 286, 102.

[122] G. de Portu, L. Micele, G. Pezzotti, *Comp. B* **2006,** 37, 556.

[123] T. Lube, *Key Eng. Mat.* **2007,** 333, 87.

[124] F. Erdogan, *Comp. Eng.* **1995,** 5, 753.

[125] R. Danzer, M. Fellner, A. Börger, M. Damani, *Prakt. Met. Sonderb.* **2003,** 34, 451.

[126] R. W. Rice, *Adv. in Ceram.* **1988,** 22, 3.

[127] A. J. Moulson, J. M. Herbert, *Electroceramics*, Chapman & Hall, London, Weinheim, New York, Tokyo, Melbourne, Madras, **1997**.

[128] K. Uchino, (Ed: H. L. Tuller), Kluwer Academic Publishers, Boston/Dordrecht/London, **1997**.

[129] K. Uchino, *Ferroelectric Devices*, Marcel Dekker, Inc., New York, Basel, **2000**.

[130] D. R. Clarke, *J. Am. Ceram. Soc.* **1999,** 82, 485.

[131] J. Pritchard, C. R. Bowen, F. Lowrie, *Brit. Ceram. Trans.* **2001,** 100, 265.

[132] R. M. McMeeking, *Int. J. Fract.* **2001,** 108, 25.

[133] B. Balzer, M. Hagemeister, P. Kocher, L. J. Gauckler, *J. Am. Ceram. Soc.* **2004,** 87, 1932.

[134] H. Cao, A. G. Evans, *J. Am. Ceram. Soc.* **1994,** 77, 1783.

[135] T. Fett, D. Munz, G. Thun, *J. Mater. Sci. Let.* **1999,** 18, 1895.

[136] T. Fett, D. Munz, G. Thun, *J. Mater. Sci. Let.* **1999,** 18, 1899.

[137] P. Supancic, *J. Eur. Ceram. Soc.* **2000,** 20, 2009.

[138] P. Supancic, Z. Wang, W. Harrer, R. Danzer, *Key Eng. Mat.* **2005,** 290, 46.